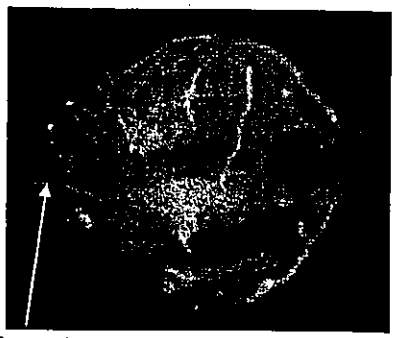

Fig. 9. Angiogram, using iodine microspheres, of extracted rabbit heart. Tube voltage and exposure time were 25 kV and 20 s, respectively.

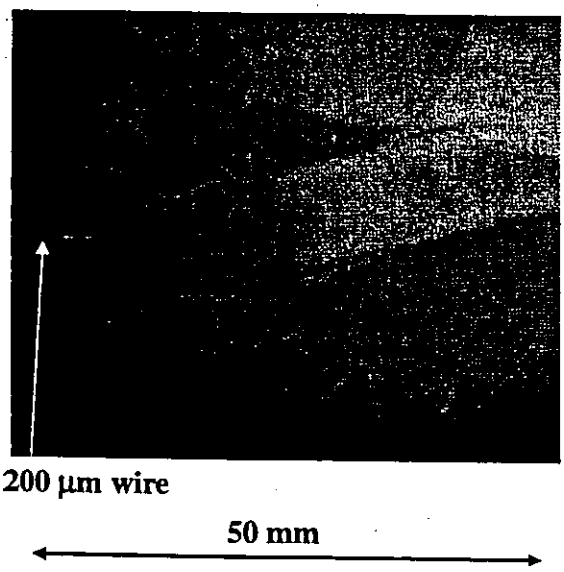

Fig. 10. Angiogram of extracted dog heart with tube voltage of 25 kV and exposure time of 60 s.

characteristic photons was approximately 4×10^6 photons/$cm^2 \cdot s$ at 1.0 m from the source with a tube voltage of 25 kV, and the photon count rate could be increased easily by increasing the tube voltage and current.

The focal spot dimensions decrease with decreasing target-cathode space, and the distance between the X-ray source and the imaging plate should be increased as much as possible to improve the spatial resolution. In soft radiography achieved with characteristic molybdenum K-series X-rays, because an X-ray lens such as a polycapillary plate[18] can be employed, the spatial resolution may be improved by decreasing the inner capillary diameter.

Under the pulsed operation, the high-voltage durability increases substantially, and both the size of the X-ray tube and the diameter of the high-voltage coaxial cable can be decreased. In this case, because the time-average tube current is regulated by the pulse repetition rate, both the tube voltage and the current can be controlled without using a hot cathode.

Recently, we developed a cerium-target X-ray tube to perform enhanced K-edge angiography utilizing cerium Kα rays (34.6 keV), since the rays are absorbed effectively by iodine-based contrast media with a K-edge of 33.2 keV. In addition, Kα rays from ytterbium (52.0 keV), tantalum (57.1 keV), and tungsten (58.9 keV) targets are very useful for performing K-edge angiography using gadolinium-based contrast media with an edge of 50.2 keV. Hence, using these rays, because the absorbed dose can be decreased effectively, extremely low-dose angiography can be accomplished.

Acknowledgment

This work was supported by Grants-in-Aid for Scientific Research (13470154, 13877114, and 16591222) and Advanced Medical Scientific Research from MECSST, Grants from Keiryo Research Foundation, The Promotion and Mutual Aid Corporation for Private Schools of Japan, JST, NEDO, and MHLW (HLSRG, RAMT-nano-001, RHGTEFB-genome-005, and RGCD13C-1).

1) A. C. Thompson, H. D. Zeman, G. S. Brown, J. Morrison, P. Reiser, V. Padmanabahn, L. Ong, S. Green, J. Giacomini, H. Gordon and E. Rubenstein: Rev. Sci. Instrum. **63** (1992) 625.
2) H. Mori *et al.*: Radiology **201** (1996) 173.
3) K. Hyodo, M. Ando, Y. Oku, S. Yamamoto, T. Takeda, Y. Itai, S. Ohtsuka, Y. Sugishita and J. Tada: J. Synchrotron Rad. **5** (1998) 1123.
4) T. J. Davis, D. Gao, T. E. Gureyev, A. W. Stevenson and S. W. Wilkins: Nature **373** (1995) 595.
5) A. Momose, T. Takeda, Y. Itai and K. Hirano: Nature Medicine **2** (1996) 473.
6) M. Torikoshi, T. Tsunoo, M. Sasaki, M. Endo, Y. Noda, T. Kohno, K. Hyodo, K. Uesugi and N. Yagi: Phys. Med. Biol. **48** (2003) 673.
7) F. E. Carroll, M. H. Mendenhall, R. H. Traeger, C. Brau and J. W. Waters: Am. J. Roentgenol. **181** (2003) 1197.
8) R. Germer: J. Phys. E: Sci. Instrum. **12** (1979) 336.
9) E. Sato, H. Isobe and F. Hoshino: Rev. Sci. Instrum. **57** (1986) 1399.
10) A. Shikoda, E. Sato, M. Sagae, T. Oizumi, Y. Tamakawa and T. Yanagisawa: Rev. Sci. Instrum. **65** (1994) 850.
11) K. Takahashi, E. Sato, M. Sagae, T. Oizumi, Y. Tamakawa and T. Yanagisawa: Jpn. J. Appl. Phys. **33** (1994) 4146.
12) E. Sato, K. Takahashi, M. Sagae, S. Kimura, T. Oizumi, Y. Hayasi, Y. Tamakawa and T. Yanagisawa: Med. & Biol. Eng. & Comput. **32** (1994) 289.
13) E. Sato, Y. Hayasi, R. Germer, E. Tanaka, H. Mori, T. Kawai, T. Ichimaru, S. Sato, K. Takayama and H. Ido: J. Electron Spectrosc. & Related Phenom. **137–140** (2004) 713.
14) E. Sato, Y. Hayasi, R. Germer, E. Tanaka, H. Mori, T. Kawai, T. Ichimaru, K. Takayama and H. Ido: Rev. Sci. Instrum. **74** (2003) 5236.
15) E. Sato, Y. Hayasi, R. Germer, E. Tanaka, H. Mori, T. Kawai, H. Obara, T. Ichimaru, K. Takayama and H. Ido: Jpn. J. Med. Phys. **20** (2003) 123.
16) H. Sugie, M. Tanemura, V. Filip, K. Iwata, K. Takahashi and F. Okuyama: Appl. Phys. Lett. **78** (2000) 2578.
17) E. Sato, K. Sato and Y. Tamakawa: Ann. Rep. Iwate Med. Univ. Sch. Lib. Arts Sci. **35** (2000) 13.
18) E. Sato, Y. Hayasi, R. Germer, E. Tanaka, H. Mori, T. Kawai, T. Ichimaru, S. Sato, K. Takayama and H. Ido: J. Electron Spectrosc. Related Phenom. **137–140** (2004) 705.

21. Umemoto Y, Tsuji K, Yang FC, et al. Leptin stimulates the proliferation of murine myelocytic and primitive hematopoietic progenitor cells. Blood 1997; 90: 3438.
22. Leclercq IA, Field J, Farrell GC. Leptin-specific mechanisms for impaired liver regeneration in ob/ob mice after toxic injury. Gastroenterology 2003; 124: 1451.
23. Picard C, Lambotte L, Starkel P, et al. Steatosis is not sufficient to cause an impaired regenerative response after partial hepatectomy in rats. J Hepatol 2002; 36: 645.
24. Zhang BH, Weltman M, Farrell GC. Does steatohepatitis impair liver regeneration? A study in a dietary model of non-alcoholic steatohepatitis in rats. J Gastroenterol Hepatol 1999; 14: 133.
25. Michalopoulos GK, DeFrances MC. Liver regeneration. Science 1997; 276: 60.
26. Muller M, Jansen PL. The secretory function of the liver: new aspects of hepatobiliary transport. J Hepatol 1998; 28: 344.
27. Muller M, Jansen PL. Molecular aspects of hepatobiliary transport. Am J Physiol 1997; 272: G1285.
28. Vos TA, Ros JE, Havinga R, et al. Regulation of hepatic transport systems involved in bile secretion during liver regeneration in rats. Hepatology 1999; 29: 1833.
29. Gerloff T, Geier A, Stieger B, et al. Differential expression of basolateral and canalicular organic anion transporters during regeneration of rat liver. Gastroenterology 1999; 117: 1408.
30. Makishima M, Okamoto AY, Repa JJ, et al. Identification of a nuclear receptor for bile acids [comment]. Science 1999; 284: 1362.
31. Parks DJ, Blanchard SG, Bledsoe RK, et al. Bile acids: natural ligands for an orphan nuclear receptor [comment]. Science 1999; 284: 1365.

0041-1337/04/7703-379/0
TRANSPLANTATION

Vol. 77, 379–385, No. 3, February 15, 2004
Printed in U.S.A.

FUNCTIONAL BIOENGINEERED CORNEAL EPITHELIAL SHEET GRAFTS FROM CORNEAL STEM CELLS EXPANDED EX VIVO ON A TEMPERATURE-RESPONSIVE CELL CULTURE SURFACE

KOHJI NISHIDA,[1,3] MASAYUKI YAMATO,[2] YASUTAKA HAYASHIDA,[1] KATSUHIKO WATANABE,[1] NAOYUKI MAEDA,[1] HITOSHI WATANABE,[1] KAZUAKI YAMAMOTO,[1] SHIGERU NAGAI,[2] AKIHIKO KIKUCHI,[2] YASUO TANO,[1] AND TERUO OKANO[2,3]

Background. **Limbal stem-cell deficiency by ocular trauma or diseases causes corneal opacification and visual loss. Recent attempts have been made to fabricate corneal epithelial graft constructs, but the technology is still evolving. We have developed a novel cell-sheet manipulation technology using temperature-responsive culture surfaces to generate functional, cultivated corneal epithelial cell sheet grafts.**

Methods. **Human or rabbit limbal stem cells were cocultured with mitomycin C -treated 3T3 feeder layers on temperature-responsive culture dishes at 37°C. Cell sheets were harvested from the dishes after 2 weeks by reducing temperature to 20°C. Histologic analyses, immunoblotting, and colony-forming assay were performed to characterize the cell sheets. Autologous transplantation was undertaken to reconstruct the corneal surfaces of rabbits with experimentally induced limbal stem cell deficiencies.**

Results. **Multilayered corneal epithelial sheets were harvested intact simply by reducing the temperature, without the use of proteases. Cell-cell junctions and extracellular matrix on the basal side of the sheet, critical to sheet integrity and function, remained intact. A viable population of corneal progenitor cells, close in number to that originally seeded, was found in the sheets. Harvested sheets were easily manipulated, transplantable without any carriers, and readily adhesive to corneal stroma so that suturing was not required. Corneal surface reconstruction in rabbits was highly successful.**

Conclusions. **Cell sheet engineering technology allows us to create intact, transplantable corneal epithelial cell sheets that retain stem cells from limbal stem cells expanded ex vivo. Our research indicates highly promising clinical capabilities for our bioengineered corneal epithelial sheet.**

Corneal epithelial stem cells reside in the basal layer of the limbus (*1, 2*), the transitional zone between cornea and bulbar conjunctiva. They govern the renewal of corneal epithelium (*3*) by generating transient amplifying cells that migrate from the limbus into the corneal basal layer (*4*). Complete loss of limbal epithelial stem cells because of severe trauma (e.g., thermal and chemical burns) or eye diseases (e.g., Stevens-Johnson syndrome, ocular pemphigoid) prompts adjacent conjunctival tissues to completely cover the cornea, leading to corneal vascularization and opacification

Regarding financial conflict of interest, Kohji Nishida and Masayuki Yamato are consultants for Cell Seed, Ltd, Tokyo, Japan and the inventor/developer designated on the patent for the presently described graft. Teruo Okano is an investor in Cell Seed, Ltd, Tokyo, Japan and an inventor/developer designated on the patent for the temperature-responsive culture surface.

This work was supported by Grants-in-Aid for Scientific Research (13470367, 13558119) of the Japan Ministry of Education, Culture, Sports, Science and Technology and The Promotion and Mutual Aid Corporation for Private School of Japan.

[1] Department of Ophthalmology, Osaka University Medical School, Suita, Japan.
[2] Institute of Advanced Biomedical Engineering and Science, Tokyo Women's Medical University, Tokyo, Japan.
[3] Address correspondence to: Kohji Nishida, Department of Ophthalmology, Osaka University Medical School, Room E7, Yamadaoka 2–2, Suita 565–0871, Japan. E-mail: knishida@ophthal.med.osaka-u.ac.jp.

Received 21 June 2003. Accepted 21 August 2003.

DOI: 10.1097/01.TP.0000110320.45678.30

with severe visual loss. Patients with limbal stem cell deficiencies can be treated with limbal transplantation (*5, 6*), but because of limited donor materials and the high risk of rejection with allogeneic transplantation, recent attempts have been made to fabricate corneal epithelium graft constructs ex vivo from expanded donor or autologous limbal stem cells on different carriers such as collagen (*7*), amniotic membrane (*8–11*), fibrin gel (*12*), and cross-linked gel of fibronectin and fibrin (*13*). Choice of carrier materials can affect the prognosis after grafting. In addition, risk of infection from these biologic materials cannot be excluded. Therefore, we now show a novel method of carrier-free cell sheet transplantation that overcomes many of these obstacles and improves the availabilities of grafting materials for this therapeutic potential.

The key to our current developments is the use of temperature-responsive cell culture surfaces. These surfaces are covalently grafted with a temperature-responsive polymer, poly(*N*-isopropylacrylamide) (PIPAAm), which facilitates cell adhesion, spreading, and growth in culture conditions at 37°C. This is above the polymer's lower critical solution temperature (LCST) of 32°C, meaning that the culture surface is dehydrated and collapsed to support cell culture. Reducing the temperature below the LCST causes the surface to rapidly hydrate and swell, prompting complete detachment of all adherent cells without typical proteolytic enzymes or EDTA treatments (*14*). Confluent cell cultures on these surfaces can then be harvested as a single contiguous cell sheet, retaining cell-cell junctions as well as deposited extracellular matrix (ECM) on the basal sheet surface (*15*). This permits the harvested cell sheets to be readily manipulated, transferred, layered, or fabricated because they adhere rapidly to other surfaces such as culture dishes (*16*) and other cell sheets (*17*). For example, stratified cardiac myocyte sheets harvested by this method rapidly integrate into multilayer tissue-like viable laminates connected to each other both physically and biochemically and exhibiting uniform synchronous pulsation (*17*).

Our approach produces robust, viable, multilayered corneal epithelial cell sheets without any substrates or carriers and promotes strong, rapid adhesion of the transplanted sheets onto corneal stroma in vivo without the need for suturing. Therapeutic advantages for this approach over current transplantation methods are considerable.

MATERIALS AND METHODS

Preparation of Cell Culture Surfaces Grafted with a Temperature-Responsive Polymer

Specific procedures for the preparation of PIPAAm-grafted cell culture surfaces (provided by Cell Seed, Ltd, Tokyo, Japan) were described previously (*16*). *N*-isopropylacrylamide monomer (kindly provided by Kohjin, Tokyo, Japan) in 2-propanol solution was spread onto polystyrene cell culture dishes (Falcon 3001, Becton Dickinson, Franklin Lakes, NJ). These dishes were then subjected to irradiation with a 0.3 MGy electron beam using an Area Beam Electron Processing System (Nissin-High Voltage, Kyoto, Japan). The PIPAAm-grafted dishes were rinsed with cold distilled water to remove non-grafted monomer and sterilized with ethylene oxide gas.

Primary Culture of Limbal Corneal Epithelial Stem Cells on Temperature-Responsive Culture Surfaces

For preparation of lethally treated National Institutes of Health (NIH)/3T3 feeder layers, subconfluent NIH/3T3 fibroblasts were incubated with 16 μg/mL of mitomycin C (MMC) for 2 hours at 37°C, then trypsinized and seeded onto 35 mm temperature-responsive culture dishes at a density of 2×10^4 cells/cm^2. We used more than 50 USA eye-bank eyes. First, we used the 7.5 mm-diameter central regions for penetrating keratoplasty. From the remaining corneoscleral rims, including limbal and peripheral regions, epithelial cells were collected by peeling off all epithelial layers after treatment with dispase II (3 mg/mL, Roche Diagnostics GmbH, Mannheim, Germany) at 37 °C for 1 hour. Collected materials were placed in trypsin/EDTA for 15 minutes to make single cell suspensions. Aliquots (1×10^4 cells/cm^2) were cultured independently of each other (i.e., cells from different eyes were not pooled) in the same dishes as lethally treated NIH/3T3 feeder layers for 2 weeks (*18*). For colony-forming assay, trypsin-EDTA treatment was used to isolate single cells from the limbal and peripheral epithelium and from corneal epithelial sheets harvested from temperature-responsive culture surfaces by reducing the temperature after 2 weeks. Cells were counted, seeded onto temperature-responsive culture surfaces (35 mm in diameter), and cultured with MMC-treated NIH/3T3 feeder layers. After 10- to 12-day cultivation, dishes were fixed and stained with rhodamine B. Colony formation was screened on the entire dish under a dissecting microscope.

Immunohistochemistry

Indirect immunofluorescence microscopy was performed using monoclonal anti-keratin 3 (AE5, Progen, GmbH, Heidelberg Germany), monoclonal anti-p63 (4A4, Santa Cruz Biotechnology, Santa Cruz, CA), and polyclonal anti-type IV collagen (Southern Biotechnology Associates, Birmingham, AL) antibodies. BrdU uptake was examined with a detection kit (no. 1296736, Roche Diagnostics, GmbH, Mannheim, Germany). Fluorescein isothiocyanate- or rhodamine-labeled secondary antibodies were from Jackson Immuno-Research Laboratories (West Grove, PA). Five specimens were examined by all the antibodies. For cross-sectional observation, 10 μm cryosections were subjected to immunostaining. In some specimens, nuclei were costained with a DNA-binding dye (Hoechst 33342, Molecular Probes, Leiden, The Netherlands) or propidium iodide (Sigma, St. Louis, MO). They were observed using a confocal laser scanning microscope (LSM-510, Zeiss, Jena, Germany).

Immunoblotting

Corneal epithelial cells were cultured on temperature-responsive culture dishes for 2 weeks. They were then recovered by one of three different methods: low temperature treatment, dispase treatment, or physical scraping with a rubber blade. All the culture in each experiment was prepared from a single donor eye. Three separate cultures from three different eyes were examined. For low temperature treatment, polymer-grafted surfaces were incubated at 20°C for 30 minutes, after which corneal epithelial cell sheets were detached. For dispase treatment, corneal epithelial cell sheets were harvested after incubation with dispase II (2.5 mg/mL, Roche Diagnostics, GmbH, Mannheim, Germany) at 37°C for 30 minutes. These were washed three times with Dulbecco's phosphate-buffered saline containing a protease inhibitor cocktail (Wako, Osaka, Japan) and 1 mM phenylmethylsulfonyl fluoride and lysed in lysis buffer (20 mM Tris-buffered saline [pH 7.4] containing 0.1% sodium dodecyl sulfate, 8 M urea, and the protease inhibitors). For physical scraping, the cell layers were removed from dish surfaces with a rubber blade in the lysis buffer. The whole cell lysates were electrophoresed on a 7.5% polyacrylamide gel with a 4.5% stacking gel on top in a discontinuous buffer system. Resolved proteins on a polyacrylamide gel were electrophoretically transferred to poly(vinylidene difluoride) (PVDF) transfer membrane (60 V for 3 hours, Immobilon-P, Millipore Corporation, Bedford, MA). The membrane was blocked with 5% bovine serum albumin fraction V and probed with either

rabbit anti-occludin polyclonal antibody (Zymed Laboratories, Inc., San Francisco, CA), mouse anti-desmocolin 3 monoclonal antibody (Dsc3-U114, Progen, GmbH, Heidelberg Germany), or mouse anti-E-cadherin monoclonal antibody (HECD-1, R&D Systems, Inc., Minneapolis, MN). Bands were detected by chemiluminescence of the product of peroxidase reaction using the ECL system (Amersham Biosciences, Buckinghamshire, UK).

Electron Microscopy

Three separate epithelial cell sheets from three different donor eyes were harvested from polymer-grafted surfaces by low temperature treatment. These were dissected, fixed in 2.5% glutaraldehyde for 2 hours, washed with cacodylate buffer, postfixed in 1.0% osmium tetroxide, and dehydrated through graded alcohols. The samples were embedded in Quetal 812 (Nisshin, Tokyo, Japan), and semithin sections (500 nm thick) were cut, stained a few seconds with toluidine blue, and observed under a conventional microscope. Ultrathin sections (90 nm), stained with uranyl acetate and lead citrate, were examined at 80 kV on a H-7000 transmission electron microscope (TEM) (Hitachi, Tokyo, Japan).

Optical Transparency of Transplantable Tissue Constructs

Three types of transplantable tissue constructs were subjected to optical transparency analysis. These were the carrier-free sheets, epithelial cells cultured on fibrin gels (*12*), or amniotic membranes (*8*). All three constructs were prepared from a single-donor cornea in each experiment, and four different sets of these constructs from four different donor eyes were examined. The average thickness of fibrin gels was 44.1±11.7 μm (SD). Amniotic membrane thickness was between 10 and 20 μm. Transmittance at 656 nm was obtained with a multichannel spectrophotometer (PMA-11, Hamamatsu Photonics, Hamamatsu, Japan). Three arbitrary points on each sample were measured. Mean±SD of four different sets of experiments were expressed. Statistical analysis was performed with one-factor analysis of variance (ANOVA) and the Bonferroni-Dunnett method.

Corneal Epithelial Cell Sheet Transplantation in a Rabbit Model

Twenty rabbits were anesthetized and underwent keratectomies of the entire corneal surface including the limbus and surgical excision of all conjunctival tissue within 5 mm of the limbus. A 7.5 mm-diameter trephine punched out the central keratectomized corneal tissue. From the remaining peripheral cornea including limbal tissue, epithelial cells were collected as described above, seeded with 1×10^3 cells/cm^2, and cultured for 3 weeks on temperature-responsive cell culture dishes. Three weeks postsurgery, the entire corneal surface of all rabbits was covered by conjunctival tissue with neovascularization, leading to severe corneal opacity. At this time, the conjunctivalized ocular surface was surgically cleared and reconstructed as outlined schematically in Figure 1. Conjunctival tissue over the cornea was surgically removed to re-expose transparent corneal stroma. Then, the bioengineered corneal epithelial sheet, fabricated in vitro from autologous corneal tissue excised at the initial surgery, was placed on the transparent stromal bed using PVDF membrane transfer. A few minutes after engrafting without suture, the PVDF membrane was simply removed, leaving the cell sheet on the stroma. Finally, the corneal surface was covered with a soft contact lens for healing protection. After surgery, topical antibiotics (0.3% ofloxacin) and steroids (0.1% betamethasone) were applied three times daily. For cell tracing, cultured corneal epithelial cells were stained with 10 nM of a fluorescent dye, PKH26 (Sigma, St. Louis, MO), in serum-free media for 30 minutes at 37°C and washed with serum-free media for 30 minutes at 37°C 1 day before transplantation. Rabbits were killed 10 days after transplantation. The cryosections of regenerated cornea were costained with a DNA-binding dye.

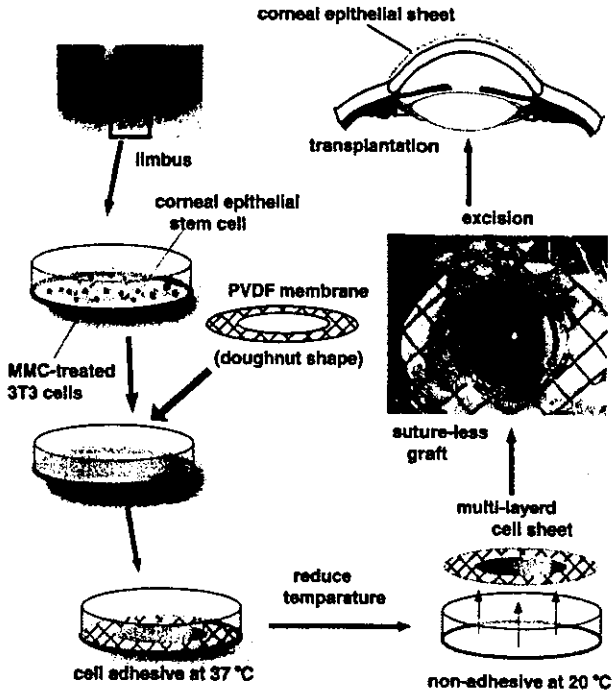

FIGURE 1. Corneal epithelial cell sheet transplantation. Limbal stem cells are collected and seeded on temperature-responsive culture surfaces. After 2 weeks in culture with a mitomycin C (MMC)-treated 3T3 feeder layer, all the multilayered cells are harvested as a cell sheet using a doughnut-shape poly(vinylidene difluoride) (PVDF) membrane after release by temperature reduction. The cell sheet is grafted onto the corneal stroma without sutures.

RESULTS

Corneal Epithelial Cell-Sheet Harvest from Limbal Stem Cell Culture on Temperature-Responsive Polymer-Grafted Culture Surfaces

To create functional bioengineered corneal epithelial sheets suitable for transplantation, we harvested human corneal limbal epithelial cells, containing corneal epithelial stem cells, from a USA eye-bank cornea (Fig. 1). These cells were seeded onto temperature-responsive culture surfaces on which MMC-treated 3T3 feeder cells had been plated 1 day previously. The outcome was highly reproducible (i.e., we always succeeded in making and harvesting cell sheets with similar morphologic characteristics). Corneal epithelial stem cells remain in the presence of feeder cell layers (*19–22*) and other specialized conditions (*23*). Under our culture conditions, epithelial cell colonies grew to reach confluency within 1 to 2 weeks. After a few additional days in culture, a multilayered corneal epithelial sheet forms spontaneously, with cells on the sheet surface exhibiting a cobblestone morphology characteristic of epithelial cells (Fig. 2a). Corneal epithelial cell phenotype was confirmed by immunohistochemistry with an anti-keratin 3 antibody specific for corneal epithelial cells (*1*, *24*) (Fig. 2b). BrdU-uptake was observed in a small portion of cells (Fig. 2c). These multilayered corneal epithelial cells could be harvested as a transplantable cell sheet

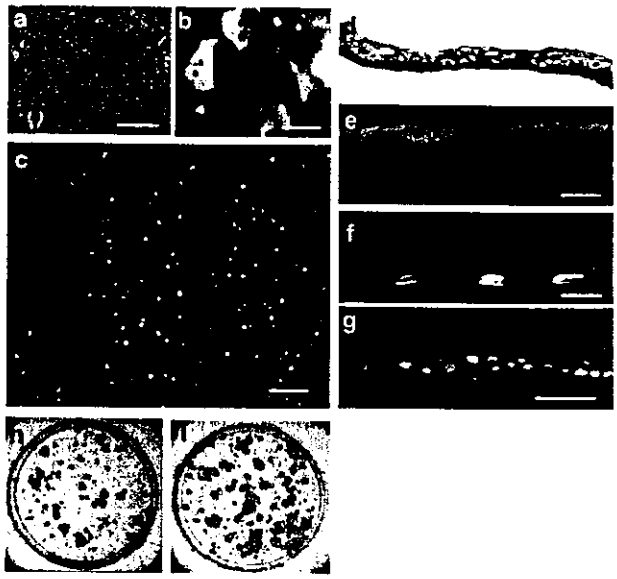

FIGURE 2. Cultured and harvested human corneal epithelial cell sheets. Phase contrast micrograph (a), anti-keratin 3 staining (b), and anti-BrdU staining (green in c) of human corneal epithelial cells cultured on temperature-responsive culture dishes. Hematoxylin eosin (d), anti-keratin 3 (green in e), anti-BrdU (green in f), and anti-p63 (green in g) staining of human corneal epithelial cell sheets harvested by reducing temperature treatment. Nuclei were costained with propidium iodide (red in c, e to g). Colony-forming assay of primary (h) and secondary culture (i). Scale bars: 50 μm in a, b and g; 100 μm in c; 20 μm in e and f.

simply by reducing culture temperature to 20°C, without use of proteases or EDTA. Harvested sheets, flattened on their basal and apical surfaces, comprised three to five cell layers with small basal cells, flattened middle cells, and polygonal flattened superficial cells (Fig. 2d). Such morphologic characteristics are similar to human corneal epithelium in vivo to some extent but are less mature and differ in that the multilayer characteristics seemed to vary depending upon location, and basal cells tended to be flattened, not cuboidal, especially in regions with fewer layers. Interestingly, only the flattened superficial cells expressed keratin 3 (Fig. 2e), whereas BrdU uptake was detected in some basal cells (Fig. 2f). p63, which has recently been proposed as a corneal epithelial stem cell marker (25), was expressed continuously in the basal cells of cell sheets (Fig. 2g). Immunostaining patterns of keratin 3 and p63 are highly similar to those in native limbal epithelium. These observations imply that epithelial stem cells were localized in the basal layer of harvested cell sheets, and differentiated epithelial cells migrated to surface layers as in vivo.

Preservation of Colony-Forming Progenitor Cells in Bioengineered Cultivated Human Corneal Epithelial Sheet

The colony-forming efficiency of the primary cultures was 4.0±2.5% (mean±SD, n=8) for our tissues that had a mean storage time in Optisol of 5.6 days (Fig. 2h). Harvested progenitor cells retained a colony-forming capacity in cell sheets harvested by temperature reduction after 2 weeks in culture (191.2±163.5% (mean±SD) of the primary culture (n=8) (Fig. 2i). This result is significant for the tissue-engineering potential of the viable sheet constructs.

Preservation of Cell-Cell Junctional Structures and Adhesive ECM in Bioengineered Human Corneal Epithelial Sheet after Harvest by Reducing Temperature Treatment

TEM revealed numerous small microplicae and microvilli in the apical cell membranes of superficial cells (Fig. 3, a and b). Also, prominent filamentous glycocalyx was evident. This structure is important for proper visual function because it is intimately associated with the mucus of the tear film layer. Tight junctions were found between lateral membranes of the apical cells, but these appeared less numerous than in vivo. Prominent desmosomes were observed along cell-cell junctions of middle cells. Interestingly, basal cells retained a continuous basement membrane-like linear deposition, although the normal complement of hemidesmosomes was not evident. Immunohistochemical analyses indicate a continuous, thick deposition of type IV collagen in sheets recovered by low temperature harvest, but faint discontinuous deposition is observed in the cell sheets harvested by dispase treatment (Fig. 4, a and b). Immunoblotting revealed that dispase treatment degraded cell-cell junctional proteins including occludin, a tight junction component, E-cadherin, and desmocolin 3, desmosomal components (Fig. 4c). These were maintained during the alternative low temperature harvest.

Transparency of Bioengineered Human Corneal Epithelial Sheet

Optical transparency was compared among the carrier-free cell sheets (n=4) and two transplantable constructs using fibrin gels (n=4) and amniotic membranes (n=4) on which corneal epithelial multilayer cells were developed, as described previously (Fig. 5). Statistical analysis revealed significant differences in light transmission measured by spectrophotometry between the cell sheet architecture and the previously reported corneal epithelial constructs. No significant difference was observed between the fibrin gel and amniotic membrane-carrier constructs.

Corneal Cell Sheets Engrafted In Vivo

We performed autologous corneal transplantation (n=20) with a rabbit model commonly used for human ocular surface

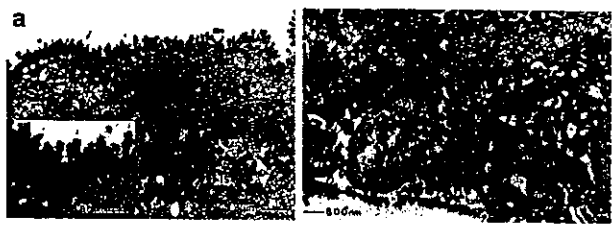

FIGURE 3. Harvested human corneal epithelial cell sheets. Apical (a) and basal surfaces with linear basement membrane-like materials (b) of harvested human corneal epithelial cell sheets. Tight junctions (*single arrow*), desmosomes (*double arrows*). Inlet shows the apical membrane with glycocalyx (*single arrows*) at higher magnification. gly, glycogen granules; mv, microvilli; IS, intercellular space; m, mitochondria; *, basement membrane-like material.

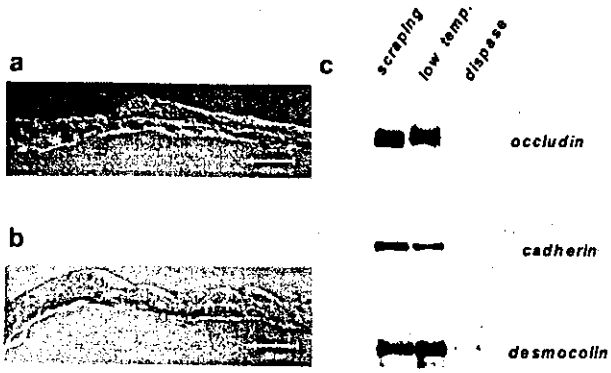

FIGURE 4. **Preservation of basement membrane and cell-cell junctional molecules. Anti-type IV collagen staining of corneal epithelial cell sheets harvested by the present method (a) and with dispase (b). (c) Western blotting with anti-occludin, anti-E-cadherin, and anti-desmocolin 3 antibodies of cell sheets recovered from temperature-responsive culture dishes by scraping, low temperature treatment, or dispase treatment.**

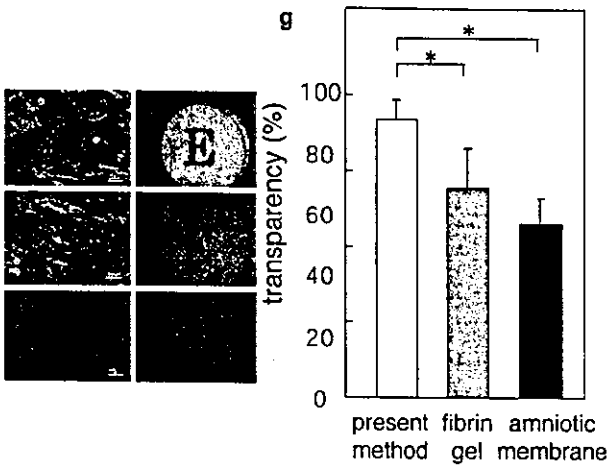

FIGURE 5. **Optical transparency of transplantable constructs. Phase contrast micrographs (a, c, and e) and macroscopic views (b, d, and f) of typescript beneath the present carrier-free construct (a and b), constructs using fibrin gel (c and d) and amniotic membrane (e and f). (g) Optical transparency (n=4, mean±SD) at 650 nm of the present carrier-free construct (*white column*), constructs using fibrin gel (*gray*), and amniotic membrane (*black*). *$P<0.01$.**

disease with limbal stem cell deficiency (*26, 27*). The procedure involves a keratectomy of the entire corneal surface, including the limbus, and excision of the entire conjunctival tissue within 5 mm of the limbus for complete loss of the corneal and limbal epithelium, including corneal stem cells. Three weeks after surgery, conjunctival scar tissue with vascularization from migrating conjunctival cells covered the entire corneal surface, leading to severe corneal opacity. This is the expected result without intervention. For grafting experiments, the conjunctivalized ocular surface was surgically modified again (Fig. 6a). First, conjunctival scar tissue on the cornea was surgically removed to re-expose the native, transparent corneal stroma. Then, cultured, autologous, multilayered corneal epithelial cell sheets were harvested by reducing temperature using a PVDF membrane with an outer diame-

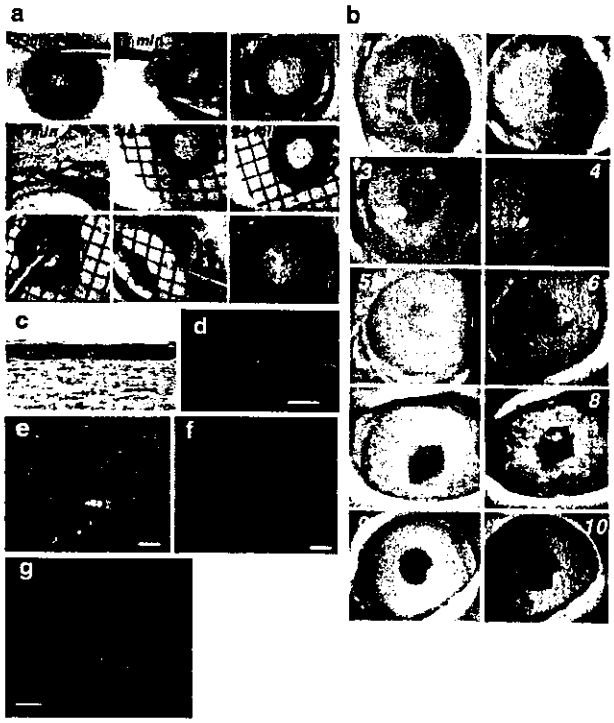

FIGURE 6. **Regeneration of rabbit corneas by the autologous transplantation of bioengineered corneal epithelial cell sheets. (a) Serial photographs of the transplantation procedures. Labeling indicates approximate time stage. Three weeks postsurgery of keratectomy, including the limbus, the entire corneal surface was covered by conjunctival tissue with neovascularization (photograph at 0 min). Conjunctival tissue over the cornea was surgically removed to re-expose transparent corneal stroma (5 min and 10 min). Then, the bioengineered corneal epithelial sheet was harvested from temperature-responsive culture dishes using a supporter (15 min) and placed on the stromal bed (16 min). The sheet readily adhered to corneal stroma in a few minutes without suture (20 min), and the PVDF membrane was simply removed (21 min and 25 min), leaving the cell sheet on the stroma (30 min). (b) Treated eyes were examined without (*1, 3, 5, 7, 9*) or with fluorescein (*2, 4, 6, 8, 10*) before transplantation (*1, 2*), immediately after transplantation (*3, 4*), and 10 days (*5, 6*), 30 days (*7, 8*), and 180 days (*9, 10*) after transplantation. Green fluorescence resulted from the loss of functional epithelial barrier. (c) Hematoxylin eosin stained section of the regenerated cornea 3 weeks after transplantation. (d) Double staining of keratin 3 (red) and nuclei (blue) of the regenerated cornea 3 weeks after transplantation. (e and f) Cultured corneal epithelial cells were stained with a cell-tracer (red) 1 day before harvest. (g) The regenerated cornea 10 days after transplantation of the sheet that had preoperatively been stained with a cell-tracer (red) was stained with a DNA-binding dye (blue) after sectioning. Scale bars: 50 μm in c, d and e, f; 20 μm in g.**

ter of 30 mm and 12 mm-diameter hole punched out of its center. This PVDF geometry permits sufficient support for cell sheet harvest while suspending a central portion of the epithelial sheet freely across the 12 mm-diameter central opening. This unique configuration conveniently allows application of a 12 mm-diameter corneal sheet construct directly onto the surgically prepared corneal surface. The intact multilayered corneal sheet was placed directly over the bare corneal stroma. After 5 minutes of contact after placement, the sheet had readily adhered to the underlying corneal stroma, self-stabilizing without any suturing. The PVDF membrane was then excised.

Immediately after surgery, fluorescein staining showed that the corneal epithelial sheet covered the entire corneal surface homogeneously, reflecting a successful procedure (Fig. 6b). The next day, the graft remained firmly attached to the corneal surface, with some ocular surface inflammation seen. During postoperative healing, ocular surface inflammation subsided, and corneal transparency was restored. During observation periods of up to 180 days, all bioengineered corneal sheet grafts remained stable at the initial placement site, covering the entire corneal surface. The corneal epithelium regenerated by corneal sheet graft healing exhibited a normal appearance, with slightly thin corneal epithelium, cuboidal basal cells, and flattened medial and superficial cells (Fig. 6c). All the epithelial cell layers expressed keratin 3 in each of two regenerated corneas examined by immunohistochemistry (Fig. 6d).

To follow the transplanted corneal epithelial cells after grafting, transplanted cells were stained with a cell-tracer red dye 1 day before surgery (Fig. 6, e and f). Later, the entire thickness of the regenerated corneal epithelium exhibited red fluorescence (Fig. 6g), indicating that the regeneration originated with the transplanted cells.

DISCUSSION

Clinical applications of cultivated corneal epithelial cell transplants are of increasing interest because of burgeoning therapeutic needs. Several trials have been reported to date (*8–10, 12, 28*), but several compelling appear to remain. Pellegrini et al. (*28*) initially reported the possibility of the clinical use of corneal epithelial cell sheets. At that time, these were harvested by dispase treatment from culture dishes. Results from the present study show that such proteolytic treatment upon harvest causes marked degradation of cell-cell junctional and ECM proteins, and cell sheets recovered by proteolytic treatment appear to be suboptimal in their adherence to integration with the cornea. In later work, Pellegrini's group switched their method to fibrin gel carriers in an attempt to overcome this problem (*12*).

After Pellegrini's initial report, several investigators reported transplantation of cultivated corneal epithelial cells using carriers such as amniotic membrane (*8–11*) and fibrin gel (*12*) without the use of dispase. In these methods, limbal epithelial cells are cultivated on the carrier, and the resultant constructs, composed of both epithelium and carrier, are transplanted onto the cornea with suturing. Although these methods provide easy handling of the constructs, posttransplant effects from the carrier are expected to influence the clinical outcome, namely corneal transparency and graft survival, postoperatively. Postoperative observations in many cases showed that the amniotic membrane carriers permanently stay between grafted epithelial layers and the corneal stroma, with only loose attachment to corneal stroma. Alternatively, fibrin gel is an attractive carrier for keratinocyte-sheet transplantation, but unlike its application to skin, the gel on the cornea must be resolved completely without any scarring. Even microtrauma or subtle inflammation often leads to corneal opacity with fibrin. Suboptimal performance leading to poor transplant integration and healing is therefore expected to cause some corneal opacification.

In the present study, we show that viable, intact, multilayered corneal epithelial cell sheets can be conveniently produced from limbal stem cells expanded ex vivo on polymer-grafted temperature-responsive cell culture surfaces. Histologic and biochemical analyses clearly demonstrate a well-structured, compact multilayered cell sheet architecture, with the expected native cell microstructures such as microvilli, tight junctions, desmosomes, and basement membrane similar to those in native corneal tissue. Neither destructive proteolytic enzymes nor EDTA are required for cell sheet harvest, and thus cell-cell junctions and basal ECM critical to sheet integrity and function remain intact in our harvested cell sheets. As a result, the sheets are easily manipulated and readily adhesive to tissue and material substrates using endogenous, intact ECM on the basal cell surface. In addition, cell sheets generated on the temperature-responsive culture surfaces retain viable corneal epithelial progenitor cells and are successfully transplantable, producing corneal surface reconstruction in a rabbit model.

Clearly, donor cell survival is a key issue for the long-term success of reconstructive surgeries using bioengineered materials and warrants further investigation. Colony-forming assay revealed a 4.0% primary colony-forming efficiency. This is lower than the 16% to 27% efficiency found by Pellegrini and associates (*29*), possibly because our cells were collected from eye bank eyes that had various death-to-preservation times (range 2.5–13 hours) with subsequent storage in Optisol for an average of 5.6 days. Other distinctions were that Pellegrini's team seeded cells from the limbus only, whereas we used those from the limbus and the peripheral cornea because of partial loss of limbal epithelium at the eye bank, and that our system used an NIH/3T3 feeder layer rather than the J2–3T3 feeder layer that is thought to promote better colonization. Preliminary work (data not shown) indicated that the use of the PIPAAm culture surface is not a factor in the primary colony-forming efficiency because cells grow as well on this as on the plastic plates normally used. A key finding from this study is the fact that cultured cell sheets retain progenitor cell populations close in number to those originally seeded. This result is of particular importance for clinical application of such sheets in transplants.

The rabbit studies showed that convenient and robust tissue transfer to the corneal surface was feasible, facilitating graft placement, stabilization, and adhesion without the trauma of sutures. Our approach also allows corneal regeneration without graft removal. The fact that transplanted sheets adhere strongly to the corneal stroma within a few minutes without sutures is likely attributable to intact ECM on the basal side of the sheet that promotes sheet-stroma integration. Analogously, we previously demonstrated that vascular endothelial cell sheets (*16*) and cardiomyocyte sheets (*17*) harvested from temperature-responsive surfaces easily adhere onto other surfaces by way of this same mech-

anism. An interesting observation here is the differential immunofluorescence of keratin 3 in the cell sheet in vitro compared with the sheet in situ. In the isolated cell sheet, only superficial keratin 3 immunolocalization was seen, whereas keratin 3 was found throughout the whole epithelium 4 weeks after grafting. We suspect that this might be caused by environmental cues in much the same way as Espana et al. (*30*) demonstrated with their identification of keratin 3 in limbal cells when grown in organ culture in the center of a debrided cornea. Further investigation of this mater is planned.

On the basis of the above results from animal experiments, we have recently initiated clinical application of our cell sheet transplantation approach to regenerate damaged ocular surface. So far, we performed the same surgical techniques as those used in the animal experiments in four patients with limbal stem cell deficiencies. Two grafts were allogenic, one autologous and one living-related (mother donor). For the autologous and living-related surgeries, cell sheets were generated from 5×10^3 cells/cm^2 obtained from a 1 to 2 mm^2 limbal biopsy. But because stored tissues were being used for the allogenic surgeries, we seeded twice as many cells (1×10^4 cells/cm^2). Despite the short-term observation periods (6 months, 5.5 months, 3 months, and 2 months), bioengineered corneal sheet grafts remained stable, covering the entire corneal surface. In all cases, corneal transparency was recovered and visual acuity restored.

In summary, cell sheet engineering techniques using temperature-responsive culture surfaces permit the rapid attachment of an intact corneal epithelial sheet without any carriers or sutures. With the present method, the entire corneal surface remains completely covered by the grafted epithelial cell sheet when surgery is finished. This would minimize corneal opacification. Because no biologic materials except epithelial cells and their deposited matrix are grafted, host immunologic reaction can also be minimized. The results shown here suggest promising clinical capabilities for a bioengineered corneal sheet that is ideal for transplantation. The approach overcomes a number of problems associated with other related techniques. Furthermore, the present grafting method without any carriers or sutures could, in principal, be applied to corneal endothelial cells as well as retinal pigmented epithelial cells. Such cell sheets harvested from temperature-responsive culture dishes should enable further functional and histologic tissue replacement by way of integration with host tissues.

Acknowledgments. The authors thank Professor D. W. Grainger (Colorado State University) and Professor A. J. Quantock (Cardiff University, UK) for the useful comments and technical criticism and Y. Ishii (New Vision, Co. Ltd.) for technical assistance.

REFERENCES

1. Schermer A, Galvin S, Sun TT. Differentiation-related expression of a major 64K corneal keratin in vivo and in culture suggests limbal location of corneal epithelial stem cells. J Cell Biol 1986; 103: 49.
2. Cotsarelis G, Cheng SZ, Dong G, et al. Existence of slow-cycling limbal epithelial basal cells that can be preferentially stimulated to proliferate: implications on epithelial stem cells. Cell 1989; 57: 201.
3. Thoft RA, Friend J. The X, Y, Z hypothesis of corneal epithelial maintenance. Invest Ophthalmol Vis Sci 1983; 24: 1442.
4. Buck RC. Measurement of centripetal migration of normal corneal epithelial cells in the mouse. Invest Ophthalmol Vis Sci 1985; 26: 1296.
5. Kenyon K, Tseng SC. Limbal autograft transplantation for ocular surface disorders. Ophthalmology 1989; 96: 709.
6. Tsubota K, Satake Y, Kaido M, et al. Treatment of severe ocular-surface disorders with corneal epithelial stem-cell transplantation. N Engl J Med 1999; 340: 1697.
7. Schwab I. Cultured corneal epithelia for ocular surface disease. Trans Am Ophthalmol Soc 1999; 97: 891.
8. Tsai RJ, Li LM, Chen JK. Reconstruction of damaged corneas by transplantation of autologous limbal epithelial cells. N Engl J Med 2000; 343: 86.
9. Schwab IR, Reyes M, Isseroff RR. Successful transplantation of bioengineered tissue replacements in patients with ocular surface disease. Cornea 2000; 19: 421.
10. Koizumi N, Inatomi T, Suzuki T, et al. Cultivated corneal epithelial stem cell transplantation in ocular surface disorders. Ophthalmology 2001; 108: 1569.
11. Shimazaki J, Aiba M, Goto E, et al. Transplantation of human limbal epithelium cultivated on amniotic membrane for the treatment of severe ocular surface disorders. Ophthalmology 2002; 109: 1285.
12. Rama P, Bonini S, Lambiase A, et al. Autologous fibrin-cultured limbal stem cells permanently restore the corneal surface of patients with total limbal stem cell deficiency. Transplantation 2001; 72: 1478.
13. Han B, Schwab I, Madsen T, et al. A fibrin-based bioengineered ocular surface with human corneal epithelial stem cells. Cornea 2002; 21: 505.
14. Yamada N, Okano T, Sakai H, et al. Thermo-responsive polymeric surfaces; control of attachment and detachment of cultured cells. Macromol Chem Rapid Commun 1990; 11: 571.
15. Yamato M, Utsumi M, Kushida A, et al. Thermo-responsive culture dishes allow the intact harvest of multilayered keratinocyte sheets without dispase by reducing temperature. Tissue Eng 2001; 7: 473.
16. Hirose M, Kwon OH, Yamato M, et al. Creation of designed shape cell sheets that are noninvasively harvested and moved onto another surface. Biomacromolecules 2000; 1: 377.
17. Shimizu T, Yamato M, Isoi Y, et al. Fabrication of pulsatile cardiac tissue grafts using a novel 3-dimensional cell sheet manipulation technique and temperature-responsive cell culture surfaces. Circ Res 2002; 90: e40.
18. Lindberg K, Brown ME, Chaves HV, et al. In vitro propagation of human ocular surface epithelial cells for transplantation. Invest Ophthalmol Vis Sci 1993; 34: 2672.
19. Rheinwald JG, Green H. Serial cultivation of strains of human epidermal keratinocytes: the formation of keratinizing colonies from single cells. Cell 1975; 6: 331.
20. Barrandon Y, Green H. Three clonal types of keratinocyte with different capacities for multiplication. Proc Natl Acad Sci U S A 1987; 84: 2302.
21. Jones PH, Harper S, Watt FM. Stem cell patterning and fate in human epidermis. Cell 1995; 80: 83.
22. Pellegrini G, Ranno R, Stracuzzi G, et al. The control of epidermal stem cells (holoclones) in the treatment of massive full-thickness burns with autologous keratinocytes cultured on fibrin. Transplantation 1999; 68: 868.
23. Grueterich M, Espana E, Tseng SC. Connexin 43 expression and proliferation of human limbal epithelium on intact and denuded amniotic membrane. Invest Ophthalmol Vis Sci 2002; 43: 63.
24. Moll R, Franke WW, Schiller DL, et al. The catalog of human cytokeratins: patterns of expression in normal epithelia, tumors and cultured cells. Cell 1982; 31: 11.
25. Pellegrini G, Dellambra E, Golisano O, et al. p63 identifies keratinocyte stem cells. Proc Natl Acad Sci U S A 2001; 98: 3156.
26. Ti S, Anderson D, Touhami A, et al. Factors affecting outcome following transplantation of ex vivo expanded limbal epithelium on amniotic membrane for total limbal deficiency in rabbits. Invest Ophthalmol Vis Sci 2002; 43: 2584.
27. Kim J, Tseng S. Transplantation of preserved human amniotic membrane for surface reconstruction in severely damaged rabbit corneas. Cornea 1995; 14: 473.
28. Pellegrini G, Traverso CE, Franzi AT, et al. Long-term restoration of damaged corneal surfaces with autologous cultivated corneal epithelium. Lancet 1997; 349: 990.
29. Pellegrini G, Golisano O, Paterna P, et al. Location and clonal analysis of stem cells and their differentiated progeny in the human ocular surface. J Cell Biol 1999; 145: 769.
30. Espana EM, Kawakita T, Smiddy R, et al. Stromal niche controls the plasticity of rabbit limbal and corneal epithelial differentiation in a tissue recombinant model [abstract]. Invest Ophtalmol Vis Sci 2003; 44: 2030.

Available online at www.sciencedirect.com
SCIENCE DIRECT®
Biomaterials 25 (2004) 2047–2053
Biomaterials
www.elsevier.com/locate/biomaterials

Cell micropatterning using photopolymerization with a liquid crystal device commercial projector

Kazuyoshi Itoga, Masayuki Yamato, Jun Kobayashi, Akihiko Kikuchi, Teruo Okano*

Institute of Advanced Biomedical Engineering and Science, Tokyo Women's Medical University, 8-1 Kawada-Cho, Shinjuku-ku, Tokyo 162-8666, Japan

Received 19 July 2003; accepted 15 August 2003

Abstract

Photopolymerization has been widely used for surface micropatterning. The technique often requires photomasks and light sources with appropriate energies or filters. For rapid prototyping of surface photo-micropatterning, we have developed a novel device by modifying a commercially available liquid crystal device projector. In place of the image expansion unit of the projector, we attached an image reduction unit, an adjustable stage, and an optical monitoring unit. The device projected computer-generated images onto surfaces and subjected these patterns to photopolymerization. Micropatterned images can be easily prepared with various software run on personal computers. With the developed photopolymerization device, micropatterning of poly(ethylene glycol) (PEG) was achieved with PEG-diacrylate and a visible light photopolymerization initiator, camphorquinone. Selective cell adhesion control was also achieved on the micropatterned surfaces.

Keywords: PEG; LCD projector; Cell patterning; Cell culture; Photopolymerization

1. Introduction

Surface micropatterning has been widely investigated for a wide range of biomedical applications from single cell manipulations in basic cell biology [1,2] to complex multi-patterned biochips [3]. Various methods have been exploited to produce reliable patterns, including micro-contact printing [4,5], laser ablation [6,7], photolithography [8–11], inkjet printing [12–14], and microscale self-assembly [15]. Except for inkjet printing and self-assembly, patterning has generally utilized photomasks and energy sources such as light and electron beams [16]. Preparation of photomasks is often time-consuming and expensive. Qin et al. showed the utilization of high quality laser printers and commercial transparency sheets for over-head projectors to prepare quality photomasks [17]. However, high resolution requires an expensive high-end laser printer. In addition, adequate light sources and optics are requisite for precise micropatterning.

In order to overcome these shortcomings, we developed a novel device by modifying a commercially available liquid crystal device projector (LCDP) for rapid photo-prototyping of micropatterned surfaces. Recent innovations have realized large-scale liquid crystal panels with a high density and micrometer scale resolution. A typical pixel size is approximately 20 μm. Such resolution can be useful for micropatterning in several biomedical fields, particularly those associated with cell patterning and arraying technologies. Furthermore, LCDP has a well-controlled light source. Projection images can be easily generated by a personal computer (PC) without any special software. Here we describe cell patterning on surfaces micropatterned with this new device.

2. Materials and methods

2.1. Materials

Poly(ethylene glycol) (PEG)-diacrylate (MW = 1000) was kindly provided by NOF Co. (Tokyo, Japan).

*Corresponding author. Tel.: +81-3-3353-8111; fax: +81-3-3359-6046.
E-mail address: tokano@abmes.twmu.ac.jp (T. Okano).

0142-9612/$ - see front matter © 2003 Elsevier Ltd. All rights reserved.
doi:10.1016/j.biomaterials.2003.08.052

3-methacryloxypropyltrimethoxysilane (MPTMS, Shin-Etsu Chemical Co., Tokyo, Japan), anhydrous methanol (Kanto Chemical Co., Tokyo, Japan), (±)-camphorquinone, *N,N*-dimethyl-*p*-toluidine, anhydrous 1,4-dioxane (Wako Pure Chemical Industries, Ltd., Osaka, Japan), and all other chemicals were used as received. An LCDP (LP-SG7) was kindly provided by SANYO Electric Co. (Osaka, Japan). A objective lens having long working distance (M Plan Apo, 2×, N.A. 0.055) and a tube lens (MT-40) were purchased from Mitutoyo Co. (Kanagawa, Japan).

2.2. Functionalization of glass surfaces

Both sides of cover glass slips (24 × 50 mm, 0.2 mm in thickness, Matsunami Glass Inc., Japan) were treated by oxygen plasma (irradiation intensity: 400 W, oxygen pressure: 0.1 mmHg) for 180 s in a plasma dry cleaner (PX-1000, SAMCO International, Kyoto, Japan) to clean the surfaces. Plasma-treated coverslips were installed in a separable flask, and dried under vacuum for 30 min. Ten milliliters of MPTMS and 500 ml of anhydrous methanol were poured into the flask under nitrogen gas. The coupling reaction of MPTMS with clean, dry coverslip surfaces proceeded under reflux for 24 h at 60°C. The modified coverslips were rinsed repeatedly with methanol and distilled water, and dried for 24 h at 70°C.

2.3. Surface patterning of PEG derivatives by photopolymerization

Surface patterning of PEG derivatives on the coverslip was performed by irradiation of visible light through patterned images on the liquid crystal panel. A typical preparation procedure follows: PEG-diacrylate (0.60 g), camphorquinone (20 mg) as a photopolymerization initiator [18,19], and *N,N*-dimethyl-*p*-toluidine (2.0 μl) as photosensitizer were dissolved in 0.80 g of 1,4-dioxane. The solution (4.0 μl) was dropped on the MPTMS-immobilized coverslip. This solution was then covered with an untreated coverslip (24 × 24 mm), creating a liquid film spread uniformly between the coverslips. The approximate thickness of the solution between coverslips is ~7 μm. The set of coverslips was placed in the LCDP apparatus where the MPTMS-immobilized coverslip was the front side toward the light source. Visible light irradiation was performed directly through the top of the MPTMS-immobilized coverslip for 20 min. After irradiation, the untreated coverslip was stripped off from the microfabricated PEG immobilized on the MPTMS-immobilized coverslip. The resulting PEG-micropatterned coverslip was repeatedly washed with acetone and further characterized.

2.4. Characterization of LCDP photo-patterned surfaces

Micropatterned surfaces were examined under a phase contrast microscope (ET-300, Nikon, Tokyo, Japan) and a scanning electron microscope (S-800, Hitachi, Tokyo, Japan). For electron microscopy, micropatterned surfaces were deposited by a thin conducting gold sputtered layer. Three-dimensional profiles of the surfaces were obtained by reflective confocal laser scanning microscopy (ICM-1000, Leica Microsystems, Wetzlar, Germany) and Tapping mode® atomic force microscopy (AFM) (Nano Scope IIIa, Digital Instruments, Santa Barbara, CA). Micropatterned surfaces were stained with a hydrophobic fluorescent dye, DiIC18 (Molecular Probes, Eugene, OR), at concentration of 25 μg/ml for 20 min, and washed with distilled water. Fluorescence images on DiIC18-stained micropatterned surfaces were obtained with a microscope equipped with an epifluorescence unit.

2.5. Cell culture

Bovine aortic endothelial cells (JCRB0099) were provided from Japan Health Science Foundation and cultured in Dulbecco's modified Eagle's minimum essential medium (DMEM) supplemented with 10% fetal bovine serum (FBS), 100 units/ml penicillin and 100 μg/ml streptomycin. Before cell seeding, micropatterned surfaces were incubated with fibronectin solution (50 μg/ml in Dulbecco's phosphate buffered saline, pH 7.4) at 37°C overnight and then washed. Endothelial cells (5.0×10^4 cells/ml) were seeded on these treated glass coverslips. Cell morphology in culture was monitored under a phase contrast microscope (ET300, Nikon, Japan).

3. Results

3.1. PC-controlled photopolymerization system

Typically a commercial LCDP connected to computers generating images will automatically expand the images to project them onto a large screen. Attached adjustable lenses permit focus of the projected image. Fig. 1a shows the optical diagram of typical projectors. Light irradiated from the lamp (120 W) is decomposed though the dichroic mirror to three colors: red, green and blue. After passing through each liquid crystal panel, the three-color light beams are re-integrated again by the second dichroic mirror. Then, the integrated light is expanded with a projection lens and projected onto a surface external to the projector. For our purposes, the optical path was modified as follows (see Figs. 1b and c). In the modified LCDP unit, light illuminated from the

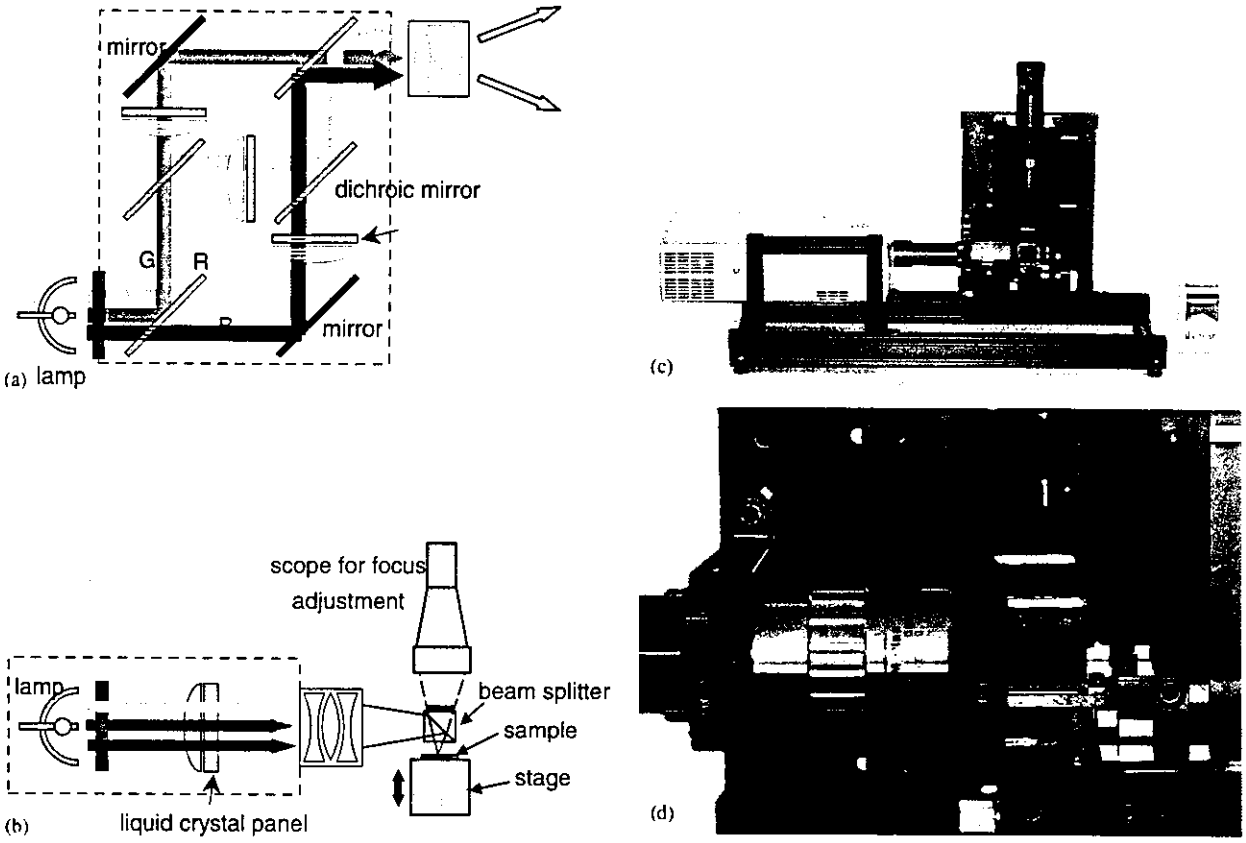

Fig. 1. Photopolymerization device. Schematic optical diagrams of LCD (a) and the modified device (b). The overall view of the device (c) and the magnified view of additional optics (d).

lamp passed through only one liquid crystal panel without light decomposition. The emitted light was down-sized by the projection lens, turned downward by the beam splitter, then irradiated onto the sample stage. For focus adjustment, the position of the sample stage was monitored and controlled (Fig. 1d). The LCDP used here has three liquid crystal panels each of 1.78 cm in diagonal consisting of 480,000 pixels (800 × 600). Each square pixel has sides of 18 μm on the liquid crystal panel, but was reduced through the projection optics. In the present study, the reduced individual pixel size was fixed to 10 μm, so that the final projection area was 8 × 6 mm. Mask patterns were generated on a typical interfaced PC with commercially available software such as Microsoft Word® and Microsoft Power Point®. The same images appearing on the PC monitor were projected onto the sample stage in a reduced size by the re-arranged internal LCDP optical path.

3.2. Micropatterned PEG graft on glass surfaces

PEG was covalently grafted onto silanated glass surfaces in order to confirm the fidelity of the surface micropatterning using the novel device. An image comprising black and white domains was used as the projected mask, although the device could also project images in an eight-bit gray scale. After photopolymerization, the resultant micropattern was easily observed under a phase contrast microscope, with generally high fidelity with the mask image generated by the PC (Fig. 2a). Each micropattern comprised small square dots having 10 μm sides. Because of the shading from embedded electronic wires aligned between pixels on the liquid crystal panel to switch each pixel on and off, small gaps were created among the square dots (arrow in Fig. 2c). Scanning electron microscopy revealed that the micro-patterned surfaces had micrometer-scale three-dimensional structures (Fig. 3). Three-dimensional profiles of the micropatterned surfaces were obtained by means of reflective confocal laser scanning microscopy and AFM (Fig. 4). The height difference was around 0.9 μm between the convex and concave domains, corresponding to white and black domains in PC-generated images, respectively.

In the present method, glass surfaces were at first treated with a surface-reactive cleaning plasma and introduced with silane-coupled double bonds prior to photopolymerization. After plasma treatment, glass surfaces were highly hydrophilic but changed to hydrophobic by the reactive silane coupling. After

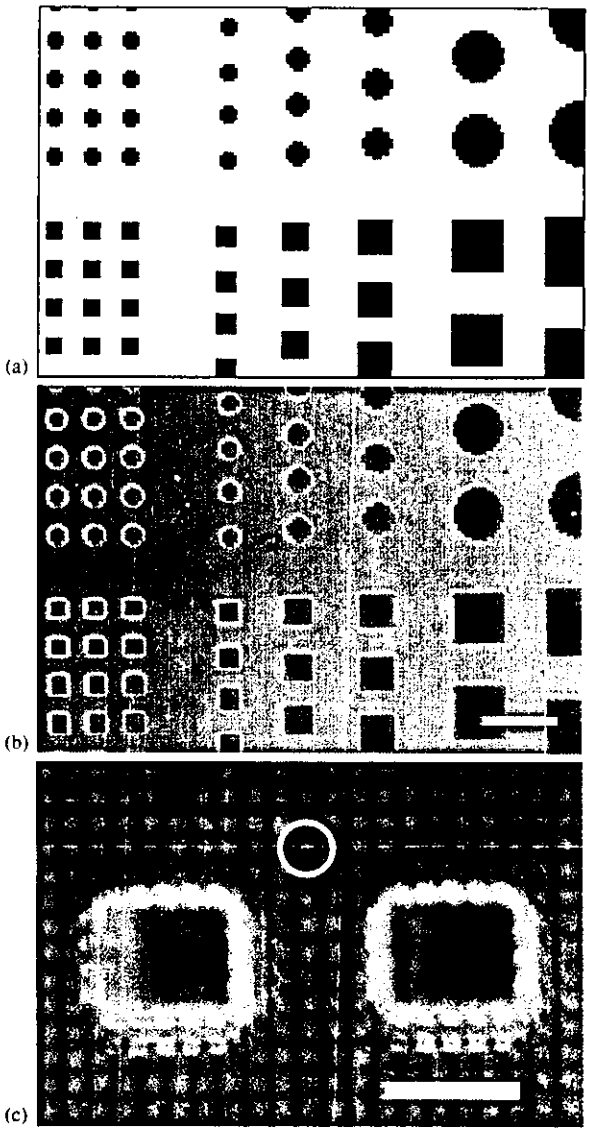

Fig. 2. Mask image generated by the PC (a), and phase contrast microscopy of micropatterned surfaces (b, c). Note small gaps among square dots (circle in (c)) Scale bar = 200 μm (b), 50 μm (c).

hydrophobic fluorescent dye (DiIC18) staining, convex patterned polymer domains corresponding to white domains in mask images showed a weak red fluorescence derived from the dye, but the concave domains corresponding to black domains in mask images did not exhibit fluorescence derived from the dye (Fig. 5). This observation strongly suggested that convex domains were slightly hydrophobic, while the concave domains were highly hydrophilic.

3.3. Micropatterned cell culture

Cell culture and in vitro adhesion experiments clearly confirmed that the surfaces formed PEG micropatterning according to exactly the original images designed

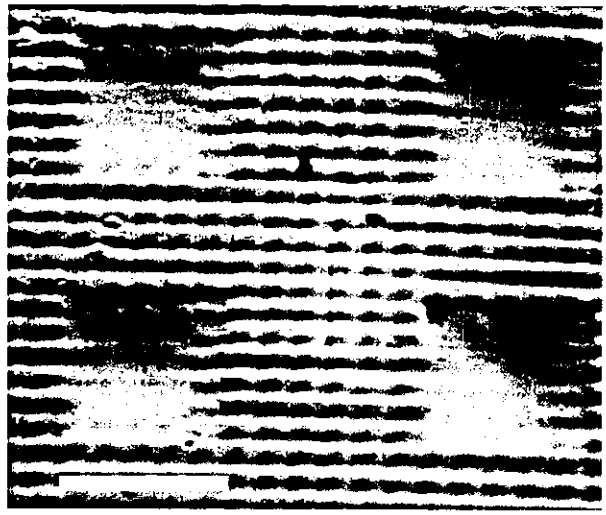

Fig. 3. Scanning electron microscopy of micropatterned surfaces. Scale bar = 50 μm.

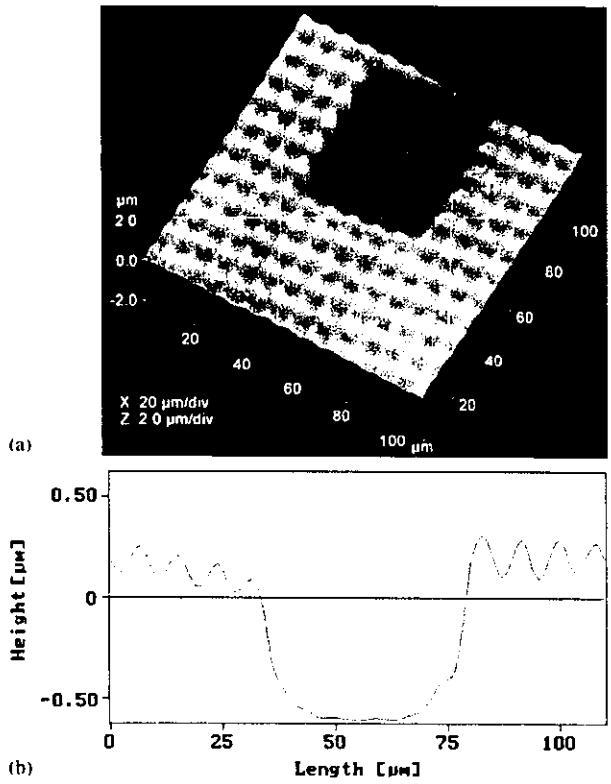

Fig. 4. Atomic force microscopy of micropatterned surface. Three-dimensional (a) and two-dimensional profiles (b).

with PC. On the silane-introduced glass surfaces, cell adhesion was hardly observed, even in the presence of serum or fibronectin (data not shown). On the micropatterned PEG surfaces, endothelial cells specifically adhered to the convex domains (Fig. 5). On the concave domains, cell adhesion was completely inhibited. Thus, micropattened cell seeding was achieved with a relatively

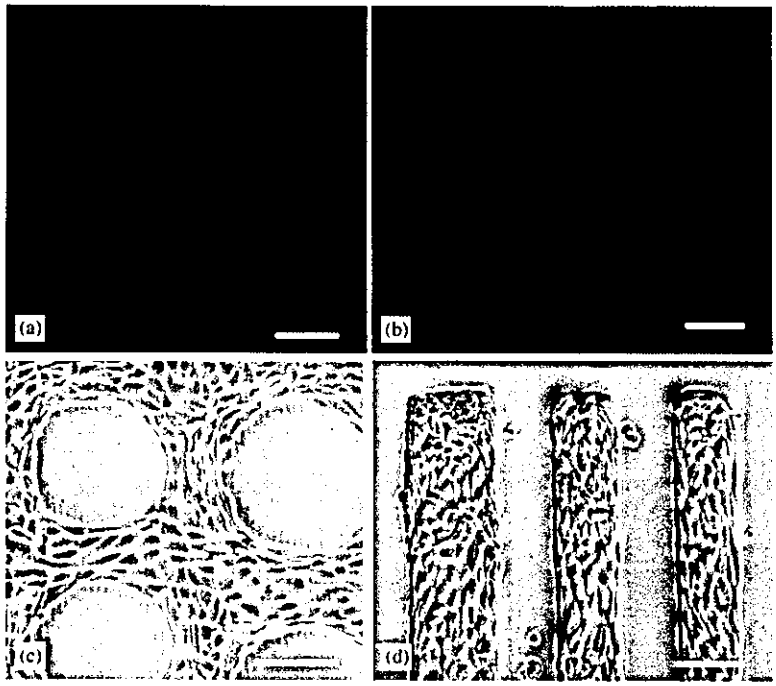

Fig. 5. Hydrophobic dye staining of micropatterned surfaces and cell culture. Micropatterned surfaces were subjected to either fluorescent staining with DiIC18 (a, b) or cells seeding (c, d). Micropatterned cell culture was microphotographed after one-day culture. Scale bar = 100 μm.

simple fabrication technique. The cell micropattern fidelity was maintained intact more than one month in the presence of serum culture. No cytotoxicity was observed during the culture (data not shown).

4. Discussion

Micro-patterned surfaces were fabricated easily and quickly with the present LCDP device without a need for expensive pattern masks, an additional light source, or other optical accessories. Even with the present typical LCDP, pattern fidelity and resolution is relevant to several biomedical applications in diagnostic arraying and microfluidics. Recent progress in high resolution and high density LCDP devices will achieve much finer micro-patterning required for other more advanced applications.

Results of the photopatterning prompt several questions about the spatial photochemistry occurring on the silane-coupled glass surfaces. From the following three lines of observation, we concluded that PEG was photo-grafted on both patterned (e.g., white and black) domains but at different degrees of polymerization under the present conditions. First, three-dimensional profiles were obtained with micropatterned surfaces. These profiles reflected the PC-generated images with high fidelity, where the white (photo-exposed) domains produced convex surface-grafted domains (Figs. 2–4) within a matrix of concave domains (non-photo-exposed regions). Vertical line topological resolution between each domain at their interface was not square, indicating some interfacial zone of continually changing topology that never reached to the glass-silane primed surface. This suggests that concave domains are covered by some photochemistry. Second, a hydrophobic fluorescent dye, DiIC18, specifically bound to the convex domains (Fig. 5). Such hydrophobic dye partitioning has been observed in many interfacial chemistry situations and is indicative of a preferred dye binding environment. Third, seeded cells selectively adhered the convex domains (Fig. 5). The concave domains repelled cells for a long time in serum-containing culture. Taken together, we assert that PEG was photo-grafted even onto the concave domains, which were masked with black domains in PC-generated images. While liquid crystal panels equipped inside the projector can completely shield emitted light to achieve black color, the irradiated light can be readily diffracted or scattered at the glass surface on both faces, within the glass substrate and between the glass sandwiching plates. Such effects could compromise the masking fidelity, permitting some light access to black-masked regions and permitting photochemistry here as well, but to a limited extend. Therefore, PEG is likely also grafted to some limited extent onto the black domains where directly irradiated light was otherwise completely shielded. Under these conditions, grafted PEG in these regions was much thinner (i.e., in the concave domains) than in the convex domains where emitted light was

irradiated directly through the liquid crystal panel at substantially higher intensity and photochemical efficiency. Molecular weight of the PEG-diacrylate used in the present study was 1000. In previous studies, protein and/or cell adhesion on PEG-grafted materials were reduced with increasing PEG molecular weight [20–22]. However, adhesion behavior on PEG-grafted surfaces has not been solely explained by PEG molecular weight effects [23]. Typical hydrogels prepared by chemical or radiation-induced procedures have cross-linking points distributed throughout the hydrogel where distances between relatively hydrophobic (e.g., acrylate or acrylamide linkages) in the gel network are spanned by relatively hydrophilic ethylene oxide chains of different lengths. By sharp contrast to previous work with longer PEG acrylates, the network structure of current grafted PEG hydrogels is considered to comprise shorter oligo-PEG acrylates where the crosslink points (hydrophobic domains) are more chemically dominant over the shorter spanning PEG chains (hydrophilic domains). Hydrophobic oligoacrylate sequences with lower PEG molecular weights would therefore be predictably exposed to adsorbing serum proteins [24,25], resulting in possibly selective adsorption of fibronectin on the convex domains. In support of this claim, hydrophobic fluorescent dye (DiIC18) was observed to selectively adsorb onto or within the convex domains. These correlative data imply that convex domains subject to intense direct LCDP irradiation are highly polymerized acrylate domains with less PEG mobility, reduced water content and generally increased local hydrophobicity capable of serum protein and dye interactions. It is plausible that the majority of the PEG was photo-immobilized at the both terminal ends to allow sufficient serum protein adsorption and subsequent cell adhesion on the convex domains. By contrast, our contention is that indirectly irradiated, less reacted PEG immobilized on the masked black regions (concave domains) maintains less crosslinking, more free terminal PEG ends, and more single-point grafting with hydrated mobility that reduces protein adsorption, and repels cells in culture.

As shown in Fig. 5, seeded cells were confined within the convex cell adhesive domains. Cells in the vicinity of edges of cell adhesive domains showed highly elongated shapes, and the cell long axis was completely parallel to the edge. To the contrary, cells in the center of cell adhesive domains did not show such a cell orientation. These findings imply that the micropattern fidelity achieved by the present method is sufficient for biomedical applications utilizing biomolecules and cells. The present LCDP device has both a liquid crystal panel imaging PC-generated patterns and a strong light source. Because of availability, cost and ease of modification to accommodate photo-patterning, such an all-in-one device should prove useful for the preparation of micro-patterned surfaces for biomedical applications in a rapid prototyping manner.

5. Conclusion

We developed an all-in-one device for photopolymerization-based surface micropatterning by modifying a commercially available liquid crystal device projector. Micropatterned surfaces were fabricated from the images prepared with various softwares run on personal computers. With PEG-diacrylate and a visible light photopolymerization initiator, camphorquinone, 10-μm resolution, which seems sufficient for biomedical applications, was obtained. On the micropatterned surfaces, selective cell adhesion control was also achieved.

Acknowledgements

The present work was supported by Grants-in-Aid for Scientific Research (13308055) of Japan Society for Promotion of Science, The Promotion and Mutual Aid Corporation for Private School of Japan, and Core Research for Evolution Science and Technology from Japan Science Technology Corporation. We also appreciate the useful comments and technical criticism from Prof. D.W. Grainger (Colorado State University, USA). We are thankful for the cooperation of Digital Systems Development Center of Sanyo Electric Co., Ltd.

References

[1] Singhvi R, Kumar A, Lopez GP, Stephanopoulos GN, Wang DIC, Whitesides GM, Ingber DE. Engineering cell shape and function. Science 1994;264:696–8.
[2] Chen CS, Mrksich M, Huang S, Whitesides GM, Ingber DE. Geometric control of cell life and death. Science 1997;276:1425–8.
[3] Jager EW, Inganas O, Lundstrom I. Microrobots for micrometer-size objects in aqueous media: potential tools for single-cell manipulation. Science 2000;288:2335–8.
[4] Mrksich M, Dike LE, Tien J, Ingber DE, Whitesides GM. Using microcontact printing to pattern the attachment of mammalian cells to self-assembled monolayers of alkanethiolates on transparent films of gold and silver. Exp Cell Res 1997;235:305–13.
[5] Patel N, Bhandari R, Shakesheff KM, Cannizzaro SM, Davies MC, Langer R, Roberts CJ, Tendler SJ, Williams PM. Printing patterns of biospecifically-adsorbed protein. J Biomater Sci Polym Ed 2000;11:319–31.
[6] Vaidya R, Tender LM, Bradley G, O'Brien II MJ, Cone M, Lopez GP. Computer-controlled laser ablation: a convenient and versatile tool for micropatterning biofunctional synthetic surfaces for applications in biosensing and tissue engineering. Biotechnol Prog 1998;14:371–7.
[7] Yamato M, Konno C, Isoi Y, Shimizu T, Kikuchi A, Okano T. Micropatterned cell arrays fabricated by combining temperature-sensitive polymer-grafting and localized laser ablation. J Biomed Mater Res, in press.

[8] Bhatia SN, Yarmush ML, Toner M. Controlling cell interactions by micropatterning in co-cultures: hepatocytes and 3t3 fibroblasts. J Biomed Mater Res 1997;34:189–99.
[9] McFarland CD, Thomas CH, DeFilippis C, Steele JG, Healy KE. Protein adsorption and cell attachment to patterned surfaces. J Biomed Mater Res 2000;49:200–10.
[10] Chen G, Imanishi Y, Ito Y. Effect of protein and cell behavior on pattern-grafted thermoresponsive polymer. J Biomed Mater Res 1998;42:38–44.
[11] Matsuda T, Sugawara T. Development of surface photochemical modification method for micropatterning cultured cells. J Biomed Mater Res 1995;29:749–56.
[12] Wilson Jr WC, Boland T. Cell and organ printing 1: protein and cell printers. Anat Rec 2003;272A:491–6.
[13] Watanabe K, Miyazaki T, Matsuda R. Growth factor array fabrication using a color ink jet printer. Zool Sci 2003;20:429–34.
[14] Klebe RJ. Cytoscribing: a method for micropositioning cells and the construction of two- and three-dimensional synthetic tissues. Exp Cell Res 1988;179:362–73.
[15] Nishikawa T, Nishida J, Ookura R, Nishimura S, Wada S, Karino T, Shimomura M. Mesoscopic patterning of cell adhesive substrates as novel biofunctional interfaces. Mater Sci Eng 1999;C10:141–6.
[16] Yamato M, Kwon OH, Hirose M, Kikuchi A, Okano T. Novel patterned cell coculture utilizing thermally responsive grafted polymer surfaces. J Biomed Mater Res 2001;55:137–40.
[17] Qin D, Xia Y, Whitesides GM. Rapid prototyping complex structures with feature sizes larger than 20 μm. Adv Mater 1996;8:917.
[18] Monroe BM, Weiner SA, Hammond GS. Mechanisms of photochemical reactions in solution. photoreduction of camphorquinone. J Am Chem Soc 1968;90:1913–4.
[19] Ziani-Cherif H, Abe Y, Imachi K, Matsuda T. Visible-light-induced surface graft polymerization via camphorquinone impregnation technique. J Biomed Mater Res 2002;59:386–9.
[20] Mori Y, Nagaoka S, Takiuchi H, Kikuchi T, Noguchi N, Tanzawa H, Noishiki Y. A new antithrombogenic material with long polyethyleneoxide chains. Trans Am Soc Artif Internal Organs 1982;28:459–63.
[21] Nagaoka S, Mori Y, Takiuchi H, Yokota K, Tanzawa H, Nishiuchi S. Interaction between blood components and hydrogels with poly(oxyethylene) chains. In: Shalaby SW, Hoffman AS, Ratner BD, Horbett HA, editors. Polymers as biomaterials. New York: Plenum Press; 1984. p. 361–74.
[22] Park KD, Suzuki K, Lee WK, Lee JE, Kim YH, Sakurai Y, Onano T. Platelet adhesion and activation on polyethylene glycol modified polyurethane surfaces. measurement of cytoplasmic calcium. ASAIO J 1996;42:M876–81.
[23] Llanos GR, Sefton MV. Does polyethylene oxide posses a low thrombogenicity. J Biomater Sci Polym Ed 1996;4:381–400.
[24] Merrill EW. Poly(ethylene oxide) and blood contact. a chronicle of one laboratory. In: Harris JM, editor. Poly(ethylene glycol) chemistry. New York: Plenum Press; 1992. p. 199–220.
[25] Drumheller PD, Hubbell JA. Densely crosslinked polymer networks of poly(ethylene glycol) in trimethylopropane triacrylate for cell-adhesion-resistant surfaces. J Biomed Mater Res 1995;29:207–15.

Control of cell adhesion and detachment using temperature and thermoresponsive copolymer grafted culture surfaces

Yukiko Tsuda,[1,3] Akihiko Kikuchi,[2,3] Masayuki Yamato,[2,3] Yasuhisa Sakurai,[1] Mitsuo Umezu,[1] Teruo Okano[2,3]

[1]*Graduate School of Science and Engineering, Waseda University, 3-4-1 Okubo, Shinjuku, Tokyo 169-8555, Japan*

[2]*Institute of Advanced Biomedical Engineering and Science, Tokyo Women's Medical University, 8-1 Kawada-cho, Shinjuku, Tokyo 162-8666, Japan*

[3]*Core Research for Evolutional Science and Technology, Japan Science and Technology Agency*

Received 15 August 2003; revised 16 October 2003; accepted 30 October 2003

Abstract: The hydrophobic monomer, *n*-butyl methacrylate (BMA) has been incorporated into thermoresponsive poly(*N*-isopropylacrylamide) (PIPAAm) to lower PIPAAm phase transition temperatures necessary for systematically regulating cell adhesion on and detachment from culture dishes at controlled temperatures. Poly(IPAAm-*co*-BMA)-grafted dishes were prepared by electron beam irradiation methods, systematically changing BMA content in the feed. Copolymer-grafted surfaces decreased grafted polymer transition temperatures with increasing BMA content as shown by water wettabilities compared to homopolymer PIPAAm-grafted surfaces. Bovine endothelial cells readily adhered and proliferated on copolymer-grafted surfaces above collapse temperature at 37°C, finally reaching confluence. Cell sheet detachment behavior from copolymer-grafted surfaces depended on the culture temperature and BMA content. In conclusion, cell attachment/detachment can be controlled to an arbitrary temperature by varying the content of hydrophobic monomer incorporated into PIPAAm grafted to culture surfaces. © 2004 Wiley Periodicals, Inc. J Biomed Mater Res 69A: 70–78, 2004

Key words: temperature responsive surfaces; poly(*N*-isopropylacrylamide); *n*-butyl methacrylate; copolymer grafting; cell culture; cell sheet

INTRODUCTION

Poly(*N*-isopropylacrylamide) (PIPAAm), a thermoresponsive polymer, has a lower critical solution temperature (LCST) at 32°C in aqueous solution.[1,2] PIPAAm is fully hydrated with an extended chain conformation below 32°C and is extensively dehydrated to become compact above 32°C. Because of its unique, reversible hydrophilic/hydrophobic property changes with temperature, many studies utilizing PIPAAm for various applications are reported, including temperature-controlled release as drug delivery systems,[2–4] aqueous chromatography systems for separations of bioactive compounds,[5–8] and bioconjugates to regulate enzymatic activities with temperature.[9–12] Additionally, we have extensively investigated the modulation of cultured cell adhesion and detachment on PIPAAm-grafted surfaces prepared by electron beam polymerization methods.[13–16] Because PIPAAm-grafted surfaces show reversible hydrophilic/hydrophobic property alterations with temperature, a variety of cells readily adhere to and proliferate on these modified surfaces dehydrated at 37°C but not to their hydrated surfaces below PIPAAm's transition temperature. Reducing cell culture temperature below 32°C permits enzyme-free recovery of confluent cultures of many cell types as a tissue-like single cell sheet maintaining cell–cell interactions and intact extracellular matrix (ECM) proteins on the cell sheet basal surfaces.[17] Thus, this thermal system is very effective for recovering adherent cells with minimal cell damage. Recovered cell sheets can be transferred and adhered onto other surfaces by using support transfer membranes.[18,19] These novel techniques represent a new method for reconstructing complex cell strata, pseudotissue, or organ-mimicking layered constructs in tissue engineering by overlaying recovered cell sheets.[20,21]

Correspondence to: T. Okano; e-mail: tokano@abmes.twmu.ac.jp

Contract grant sponsor: Grant-in-Aid for Scientific Research A from the Japan Society for Promotion of Science; contract grant number: 13308055

We also reported that successful coculture of two cell types using patterned grafting of PIPAAm onto TCPS dishes.[22,23] Culture surfaces with both thermoresponsive PIPAAm islands and thermally inert TCPS matrix seeded with hepatocytes and bovine aortic endothelial cells (BAECs) or human fetal lung fibroblasts, TIG-1 on patterned surfaces exhibit coexisting cell-dependent functional increases, which now compels us to produce improved patterned, dual thermoresponsive polymers modified surfaces for coculture. Thus, the entire surface must be covered with thermoresponsive polymers of at least two different types, adding the required different transition temperatures. IPAAm copolymerized with other hydrophilic or hydrophobic monomers permits access to copolymers with widely varied transition temperatures.[2,24–26] By modifying surfaces with these copolymers having different transition temperatures, coculture of multiple cell types and recovery of functioning cocultured cell sheets should become possible with independent temperature alteration of the hydrophobicity of each respective patterned polymer domain on binary thermoresponsive surfaces.

In the present article, we describe cell attachment/detachment control with temperature-induced alteration of surface properties with grafted copolymers. To control cell attachment/detachment on tissue culture substrates at definite temperatures, IPAAm is copolymerized with hydrophobic monomer, BMA, and grafted to TCPS surfaces by electron beam irradiation. Surface hydration, and therefore cell attachment/detachment, are shown to be controlled to arbitrary temperatures using surface-grafted copolymers varying in incorporated BMA content.

MATERIALS AND METHODS

Materials

Commercial materials used in the modification of cell culture dishes were: IPAAm, generously provided by Kohjin (Tokyo, Japan) was purified by recrystallization from *n*-hexane and dried at 25°C under vacuum; *n*-butyl methacrylate (BMA) from Tokyo Chemical Industries Inc. (Tokyo, Japan) was distilled under reduced pressure and the fraction boiling at 80°C/L mmHg was used; and 2-propanol was obtained as high performance liquid chromatography grade from Kanto Chemical Co., Inc. (Tokyo, Japan) and used as received.

Tissue culture grade polystyrene dishes (TCPS, Falcon 3001and 3002) were obtained from Becton Dickinson Labware (Oxnard, CA). Dulbecco's modified Eagle's medium (DMEM) and Ca^{2+}-, and Mg^{2+}-free Dulbecco's phosphate-buffered saline (PBS) from Sigma Chemical Co. (St Louis, MO); and fetal bovine serum (FBS) from Moregate Exports Pty. Ltd. (Bulimba, QLD, Australia). Penicillin, streptomycin as antibiotics, and trypsin-EDTA solution were obtained from Gibco Laboratories (Grand Island, NY). Bovine aortic endothelial cells (BAECs; lot No. HH JCRB0099) were obtained from Japan Health Science Foundation (Osaka, Japan). Cells were subcultured at a 1:4 ratio once a week and used between the 15th–25th passages to maintain characteristic cell functions.

Preparation of PIPAAm-grafted surfaces

PIPAAm-grafted cell culture surfaces were prepared as described elsewhere.[13] Briefly, a fixed amount of 55 w/w % IPAAm solution in 2-propanol was added and homogeneously spread to each TCPS dish and immediately irradiated with a 0.3 MGy electron beam (EB) (150 kV, under 10^{-5} Torr) using an area beam electron processing system (Nissin-High Voltage Co., Ltd., Kyoto, Japan) to polymerize and graft PIPAAm.[13] The PIPAAm-grafted dishes were extensively rinsed with cold distilled water to remove unreacted IPAAm and un-grafted PIPAAm, then thoroughly dried at 25°C under vacuum.

Preparation of poly (IPAAm-*co*-BMA)-grafted surfaces

Poly(IPAAm-*co*-BMA)-grafted surfaces were prepared by analogous electron beam polymerization. IPAAm and BMA mixed monomer solutions in 2-propanol were spread on each TCPS dish and then irradiated with the EB with identical conditions as described above. IB-grafted dishes were first washed with cold distilled water to remove unreacted IPAAm and ungrafted copolymers, then immersed in methanol for 1 day to remove unreacted BMA. These dishes were finally dried at 25°C under reduced pressure. Prepared copolymer dishes were encoded as IBX, where X denotes the mole fraction of BMA in feed.

Quantification of grafted polymers on TCPS surfaces

The amount of PIPAAm and IBX-grafted on the base TCPS dish surfaces was determined from infrared (IR) spectra using an attenuated total reflection-Fourier transform infrared spectrophotometer (ATR-FTIR, Valor-III equipped with an ATR-500M attachment, JASCO, Tokyo, Japan). Three samples each of PIPAAm-grafted and copolymer-grafted dishes were cut to 3 × 1 cm with an ultrasonic cutter (SUW30, Suzuki Motor Co., Shizuoka, Japan). Polystyrene as a base material of the modified surfaces has a strong absorption band attributed to monosubstituted aromatic rings at 1600 cm^{-1}. An absorption for amide carbonyl (amide I) of PIPAAm appears in the region of 1650 cm^{-1}.[18] The peak intensity ratio ($I_{1650/1600}$) was used to determine the amount of PIPAAm or copolymer grafted onto each surface using a calibration curve prepared for a known PIPAAm amount cast on TCPS dishes. An absorption band attributed to an

ester carbonyl of BMA appears at 1750 cm^{-1}. However, no strong absorption was acquired in this region for IB-grafted surfaces, probably due to the minute amounts of BMA incorporated. Consequently, the amount of copolymer grafted onto TCPS dishes was correlated to the identical amount of PIPAAm in the present research.

Static water contact angle measurements

Three samples each of PIPAAm-grafted, copolymer-grafted, and control TCPS dishes were cut to 3 × 1 cm to measure static water contact angles determined by the sessile drop method from 8 to 37°C with a FACE contact angle meter (Image processing type CA-X, Kyowa Interface Science, Saitama, Japan). MilliQ water was gently placed on the sample surfaces using a syringe. The contact angles were then measured after 30 s. All samples were measured more than five times and averaged.

Cell culture

Prepared dishes for cell culture use were sterilized with ethylene oxide gas. BAECs were cultured on TCPS dishes (Falcon 3002) containing 5 mL of DMEM supplemented with 10% FBS, 100 units/mL penicillin and 100 μg/mL streptomycin at 37°C under a humidified atmosphere with 5% CO_2 and 95% air. BAECs in confluent cultures were harvested from TCPS dishes by treatment with 0.5 mL of 0.25% trypsin–0.26 m*M* EDTA in PBS for 5 min and then diluted with 5 mL of DMEM to terminate enzymatic reactions. The recovered cell suspension was centrifuged at 800 rpm for 5 min with a centrifuge (RLX-105; TOMY, Tokyo, Japan) and resuspended in DMEM supplemented with 10% FBS prior to plating on grafted dishes. Cell morphology was monitored under a phase-contrast microscope (Eclipse TE300; Nikon, Tokyo, Japan) equipped with a digital camera (FinePix S1Pro, Fujifilm, Tokyo, Japan).

Temperature-dependent single cell adhesion

BAECs were seeded onto grafted PIPAAm- and IB5-grafted surfaces at a cell density of 1.0×10^4 cells/cm^2 and cultured with DMEM in the presence of 10% FBS at either 37 or 28°C. Morphologies of cultured cells were observed 24 h after seeding by phase-contrast microscopy.

Single cell detachment by low temperature treatment

BAECs were seeded onto grafted PIPAAm-, IB5-grafted, and control TCPS surfaces at a cell density of 1.0×10^4 cells/cm^2 and cultured with DMEM in the presence of 10% FBS at 37°C for 48 h. Nonadherent cells were removed by changing culture medium, then culture dishes were transferred to a CO_2 incubator set at 20°C. Remaining adherent cell numbers on each surface were counted periodically by acquiring phase contrast photographs.

Cell sheet recovery

BAECs were plated to grafted PIPAAm, IBX-grafted, and control TCPS surfaces at a cell density of 1×10^5 cells/cm^2 and cultured at 37°C. Culture medium was changed 24 h after seeding to remove nonadherent cells. After cells formed confluent monolayers on these surfaces, each plate was transferred to a CO_2 incubator set at either 28, 25, or 20°C and morphologies of cell monolayers were monitored periodically by acquiring phase contrast photographs. Areas of remaining adherent cells were measured using NIH Image (version 1.61) for the Macintosh. The area of remaining adherent cell sheets relative to *in situ* confluently cultured cell area was calculated and averaged.

RESULTS AND DISCUSSION

Surface characterization

PIPAAm and IBX were covalently immobilized to TCPS dishes by electron beam irradiation methods well described in the previous works.[13–23] In our previous report,[16] the amount of grafted PIPAAm onto TCPS dishes was known to influence thermal regulation of cell adhesion and lifting behavior. On PIPAAm-grafted surfaces with small amounts of PIPAAm (less than 1.5 μg/cm^2), cells adhere and proliferate as those on TCPS. However, they remain adherent and no cell lifting occurs even at 20°C, probably because grafted polymer hydration and subsequent surface property alterations are not sufficient to produce cell detachment at this low density. On the other hand, cells do not show either adhesion or proliferation on surfaces grafted with more than 2 μg/cm^2 of PIPAAm. In a preliminary experiment, IB3-grafted dishes were prepared with various concentration of IB monomer solution to control grafted amounts of copolymers and thus promote adequate cell adhesion/detachment with temperature alteration. Table I summarizes amounts of IB3 grafted to TCPS surfaces prepared from different monomer concentrations as determined by ATR-FTIR. Amounts of grafted polymer exceeded 2.3 μg/cm^2 at 40 and 50 w/w % feed, which is larger than that measured for PIPAAm-grafted surfaces. As expected, cell adhesion and proliferation were not observed on such surfaces grafted with more than 2.3 μg/cm^2 of polymer despite the presence of hydrophobic component, BMA [Fig. 1(d)]. However, endothelial cells adhered on IB3 surfaces

TABLE I
Grafted PIPAAm Densities as a Function of Monomer Feed Concentration

Concentration of IB3-Monomer Solution (w/w %)	Amount of Grafted PIPAAm[a] ($\mu g/cm^2$)
30	2.01 ± 0.11
40	2.34 ± 0.12
50	2.36 ± 0.06

[a]Data are expressed as the mean of three samples with standard error of mean.

grafted with 2.01 $\mu g/cm^2$ prepared from 30 w/w % of monomer solution similar to that observed on both ungrafted TCPS and PIPAAm-grafted surfaces [Fig. 1(c)]. Therefore, in following experiments, concentration of IB-monomer feed solution was fixed to 30 w/w % during electron beam irradiation to homogeneously graft similar amounts of these copolymers to TCPS dishes. Table II summarizes the amounts of PIPAAm and IB-grafted to TCPS surfaces as determined by ATR-FTIR. All prepared surfaces were grafted with approximately 2 $\mu g/cm^2$ of PIPAAm or IBX. As will be described in the cell culture section, all of these prepared surfaces showed reliable and reproducible cell adhesion and proliferation at 37°C under culture conditions.

Surface wettability changes with temperature

Surface wettability is often correlated to cell adhesive behavior on surfaces, often showing optimal values.[27–30] Temperature-dependent wettability changes of PIPAAm- and IBX-grafted surfaces were therefore investigated. Temperature variation of static contact angles for polymer-grafted surfaces was determined using the sessile drop method at temperatures ranging from 8 to 37°C; data are shown in Figure 2. All prepared surfaces were thermoresponsive: they exhibit hydrophilicity at lower temperatures and become relatively hydrophobic at higher temperature ranges. Water contact angles of the PIPAAm-grafted surfaces demonstrate relatively large hydrophilic to hydrophobic changes with small temperature increases near 32°C.[31,32] Predictably from previous copolymer solution work,[6,24–26] IBX-grafted surfaces show decreasing wettability transition temperatures with increasing BMA content in the IB copolymer compared to homopolymer PIPAAm-grafted surfaces. Distinct temperature-dependent wettability changes were observed for all IB-grafted surfaces. However, the magnitude of hydrophilic to hydrophobic changes became smaller for the copolymer surfaces with increasing BMA content. These changes originate from known solution property alterations with temperature for IB copolymers in aqueous condition.[6,24] As BMA content in the copolymer increases, hydrophobic BMA molecules interrupt the IPAAm chain sequence continuities required for cooperative transition, disrupting

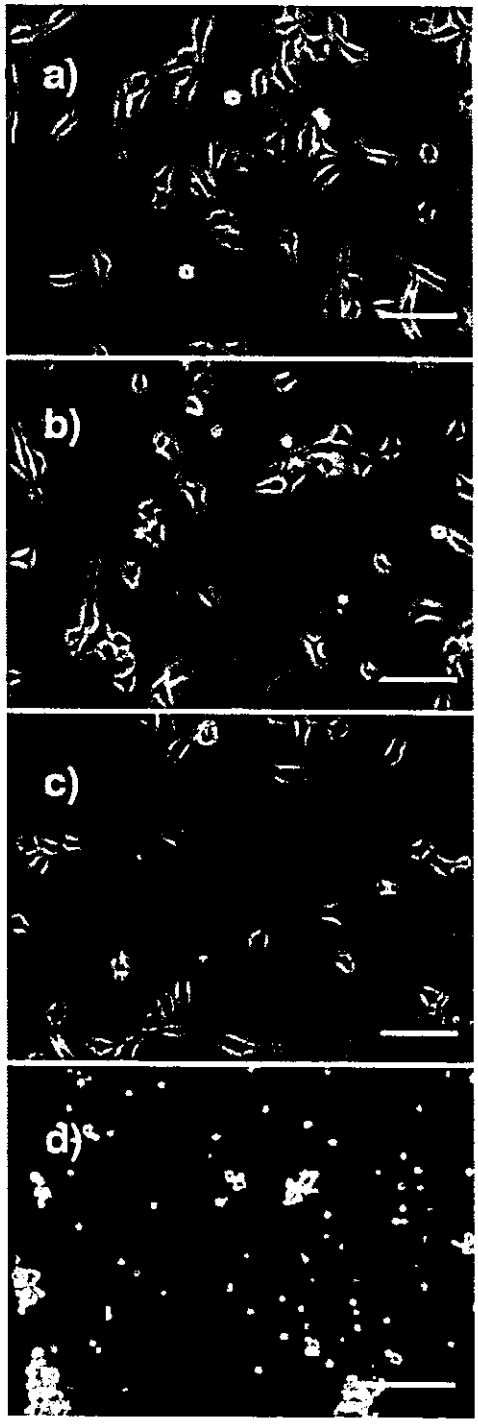

Figure 1. Cell morphologies on different IB3-grafted surfaces as a function of graft density. Grafted polymer densities measured by ATR-FTIR are: (a) 0; (b) 1.79 ± 0.01; (c) 2.01 ± 0.11; (d) 2.36 ± 0.06 $\mu g/cm^2$, respectively.

TABLE II
Grafted Polymer Densities on Prepared Surfaces Determined by ATR-FTIR

Surface	Amount of Grafted PIPAAm[a] ($\mu g/cm^2$)
PIPAAm	1.79 ± 0.01
IB1	1.80 ± 0.04
IB3	2.01 ± 0.11
IB5	2.00 ± 0.02

[a]Data are expressed as the mean of three samples with standard error of mean.

segmental cooperative effects in temperature-dependent dehydration upon temperature increases. This produces a decreased temperature sensitivity with increasing BMA composition in IB grafted copolymers. Because BMA domains in grafted IB-copolymers are hydrophobic with solubility roughly independent of temperature changes, cooperative hydration of IPAAm components in the vicinity of BMA components are suppressed. Namely, inherent meta-stability of hydration around IB-copolymers induces dehydration of IPAAm side chains with only slight temperature increases. Additionally, each hydrophobic BMA domain produces hydrophobic interactions that induce chain aggregation of BMA components. Results of temperature-dependent wettability measurements on prepared surfaces show that transition temperatures observed for grafted copolymers on TCPS dishes

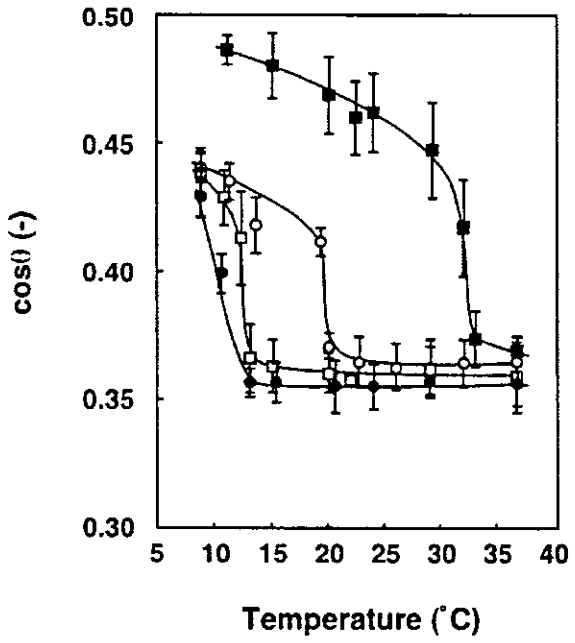

Figure 2. Temperature-dependent water contact angle changes for PIPAAm and IBX-grafted surfaces determined by sessile drop methods. Filled square, PIPAAm; open circle, IB1; open square, IB3; filled circle, IB5.

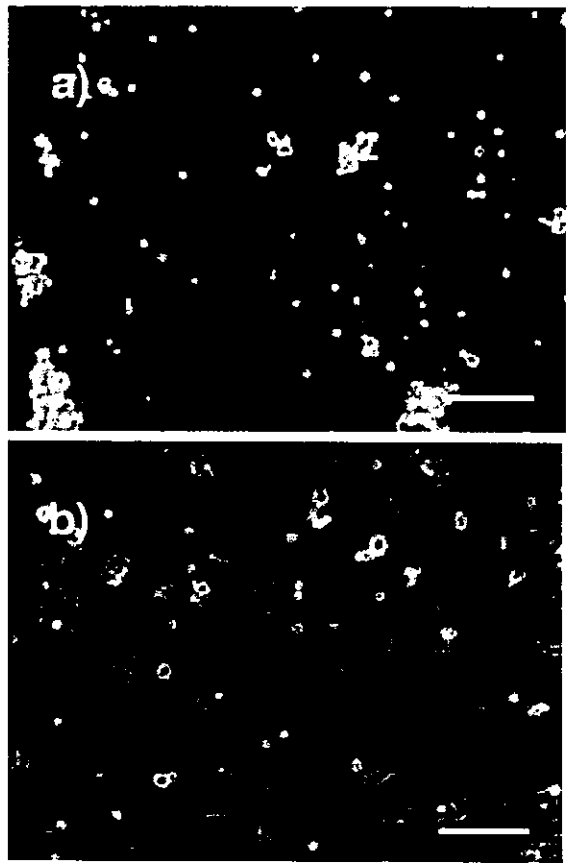

Figure 3. Microscopic views of BAECs seeded on (a) PIPAAm- and (b) IB5-grafted surfaces after 24-h culture in serum-containing media at 28°C. Scale bar: 100 μm.

are correlated to the amount of incorporated hydrophobic BMA.

Temperature-dependent single cell adhesion

Temperature-dependent cell adhesion to PIPAAm- and IB5-grafted surfaces was investigated. BAECs were sparsely seeded on prepared dishes and cultured at 28 or 37°C for 24 h in DMEM with 10% FBS. After 24-h incubation at 37°C, BAECs readily adhered and spread well on both PIPAAm- and IB5-grafted surfaces (data not shown). These results correlate with surface wettability data that both surfaces are hydrophobic at this temperature. Adherent cell numbers and morphologies were identical between PIPAAm- and IB5-grafted surfaces. By contrast, at 28°C, slightly below the transition temperature for PIPAAm, no seeded cells adhered onto PIPAAm-grafted surfaces because PIPAAm was sufficiently hydrated to suppress cell adhesion [Fig.3(a)]. Additionally, seeded cells adhered and became well spread on IB5-grafted